Accepted Manuscript

A review on recent progress of p-type nickel oxide based gas sensors: Future perspectives

Teboho P. Mokoena, Hendrik C. Swart, David E. Motaung

Please cite this article as: T.P. Mokoena, H.C. Swart, D.E. Motaung, A review on recent progress of p-type nickel oxide based gas sensors: Future perspectives, *Journal of Alloys and Compounds* (2019), doi: https://doi.org/10.1016/j.jallcom.2019.06.329.

A Review on Recent Progress of p-type Nickel Oxide Based Gas Sensors: Future Perspectives

Teboho P. Mokoena [a,b], Hendrik C. Swart [b], David E. Motaung [a,b*]

[a]DST/CSIR National Centre for Nanostructured Materials, Council for Scientific Industrial Research, Pretoria, 0001, South Africa
[b]Department of Physics, University of the Free State, Bloemfontein, ZA9300, South Africa

Abstract

Recently, technological and industrial advances uninterruptedly cause the release of hazardous and toxic gases that are harmful to human life; as a result gas sensing devices that are highly sensitive and selective to such gases are in a high demand. Presently, gas sensors based on p-type NiO are pleasing more consideration, because of its excellent reproducibility, high specific surface areas, great sensitivity, low cost and environmental friendly. Herein, we reviewed the different synthesis methods on p-type NiO nanostructures and their application as gas sensors. The fundamental gas sensing mechanism related to the p-type NiO is briefly explained. The effects of noble metals, transition metals, and transition metal dichalcogenide and phosphors materials on the NiO gas sensing performance are also discussed in detail. Influence of 0D, 1D, 2D and 3D heterostructures on NiO gas sensing characteristics are also given. The arrangement of various semiconductor metal oxides to form heterostructures which further improve the selectivity and sensitivity of the sensing parameters is also discussed and we show that number of publications on heterostructures related to NiO increased drastically since the year 2010.

Keywords: Metal oxide, Chemical sensors, NiO, Heterostructures, Nanostructures

[*]Corresponding author. David Motaung, Email: dmotaung@csir.co.za; david.e.motaung@gmail.com

Contents

1. INTRODUCTION

Rapid detection of flammable, toxic and exhaust gases are highly demanded, as many of these gases can both causes acute and health chronic effects [1, 2]. Gas detectors have been extensively utilized for monitoring of flammable, toxic and exhaust gases in an automotive industry, manufacturing production, indoor air quality and environment monitoring [3]. The reliable, low-cost, portable and low power utilization gas sensors are in a high demand due to the various applications that they

offer. Among all the existing gas sensing materials, semiconductor metal oxides (SMO) are considered to be promising materials, because of their size reliant on properties. However, the high sensitivity, low selectivity, stability, high working temperature and large power consumption are still major issues that need to be addressed [4 - 6]. In real terms, p-type SMOs have received a little attention for a long interval of time. This p-type SMO are only just beginning to be understood and therefore more studies are required on the synthesis and/or design of a greatly sensitive and selective SMO based gas sensors [7, 8].

Compared with the other SMOs, a p-type nickel oxide (NiO) with a widespread bandgap of 3.6 to 4.2 eV is the furthermost striking material because of its thermodynamically stability and unique optical, magnetic and chemical properties [9 - 11]. The gas sensing characteristics can be amplified by preparing NiO nanostructures with relatively large surface area and gas diffusion. Therefore, the change in morphology is one of the most crucial parameter that needs to be controlled during the preparation of nanomaterials [12-15]. A few examples, Lu et al. [14] reported curling porous NiO nanosheets with superior gas sensing behaviour. Miao et al. [15] studied the gas sensing features of NiO flake-flower architectures prepared via sodium dodecyl sulfonate (SDS)-hydrothermal method. These results depicted that the well-arranged flower-like NiO based gas sensor was highly sensitive and selective towards ethanol vapour. Furthermore, previous studies [16] have reported using the operando diffused-reflectance infrared Fourier transform infrared spectroscopy (DRIFT) that the water vapour in Ni doped SnO_2 based sensor generally interrelate with the Ni related surface sites such as NiO clusters or Ni atoms contained within in the SnO_2 surface lattice. They observed that the water vapour was not competing with the CO for the pre-adsorbed oxygen ions,

consequently its interfering effects in the CO sensing was significantly lessened. Pascariu et al. **[17]** studied the electrical investigation under humidity influence and they observed that $NiO–SnO_2$ nanofibers can be used as active nanostructures for humidity sensors.

Therefore, this review discusses the synthesis and/or fabrication of NiO based gas sensor nanomaterials by utilizing different synthesis techniques such as hydrothermal/solvothermal, sol-gel, chemical/co-precipitation and microemulsion methods. Furthermore, the effects of noble and transition metals (TMs), transition metal dichalcogenide (TMD), organic and phosphors materials on the NiO based gas sensors were reviewed. The influence of zero, one, two and three dimensional heterostructures on the NiO gas sensing is considered in this review. Furthermore, analysing the publications based on NiO sensors since year 2010, it is evident that the attention in heterostructures compared to undoped or doped NiO and adopted synthesis method as hydrothermal is constantly increasing on the topic.

1.1 Chemical/co-precipitation

Chemical/co-precipitation is a very efficient synthesis route for the preparation of nanopowders and/or thin films, as shown in **Figure 1a**. This synthesis method involves the two main steps which are: (i) chemical preparation route in the liquid phase, which regulates the chemical composition and (ii) heat treatment, which regulates the morphology and crystal structure **[18]**. The desired metal cations, in use as soluble salts (e.g. nitrates, oxalates, chlorides or acetates) are co-precipitated from the common medium such as hydroxides, citrates, carbonates or oxalates. The attained precipitate is dried to the desired temperature in the suitable atmosphere to form the ultimate product. In addition, the thermal decomposition of the precipitates

is relatively lesser than the ones used in the ceramic method. The difficulty in controlling of the crystal features due to quick precipitation is one of the limitations for this method **[19]**. Typical examples: Xing et al. **[20]** prepared mesoporous nickel hydroxide ($Ni(OH)_2$) with extremely large surface area with a SDS and urea as template and a hydrolysis-controlling agent, respectively. Furthermore, the $Ni(OH)_2$ was calcined at 250 ^{o}C to form NiO. During the calcination of $Ni(OH)_2$ **(Figure 1b)** at various temperatures mesoporous ball shaped NiO **(Figure 1c)** with centralized pore-size distribution, was obtained. Krishnakanth et al. **[21]** investigated the structural and magnetic characteristics of the undoped and Fe doped NiO nanoparticles prepared using a chemical/co-precipitation procedure. X-ray diffraction (XRD) revealed the increase with the crystallite size as the calcination temperature increased. Surface analyse by field emission scanning electron microscopy (FE-SEM) demonstrated the particle size reduction during the incorporation of Fe.

Fomekong et al. **[22]** studied the gas properties of Zn-doped NiO towards formaldehyde at a sub-ppm concentration level. The pure ZnO and Zn-doped NiO were effectively prepared by a thermal treatment of the resultant nickel zinc malonate previously synthesized by controlled co-precipitation in aqueous solution. Yang et al. **[23]** reported a highly sensitive NiO based sensing materials and its ultra-selective detection towards benzaldehyde gas. The remarkable improvement in responses to benzaldehyde analyte gas and rapid fast response-recover (~ 22.6 – 31.5 s) feature was observed from NiO gas sensors. Sun et al. **[24]** studied synthesis and enhanced gas sensing perfomance of NiO-decorated SnO_2 microflowers amassed with porous nanorods. The sensor was highly sensitive to 1000 ppm of ethanol gas with the response of 576.5 at the operating temperature of 320 ^{o}C. Kruefa et al. **[25]** reported enhanced p-type NiO gas sensing performances

synthesized using precipitation with RuO_2 impregnation. The results depicted relatively great response of 29.1 towards 1000 ppm of ethanol vapour at the operating temperature of 350 ^{o}C.

1.2 Sol-gel

Sol-gel procedure is one of the most powerful synthesis techniques used for developing metal oxides (MOX) on a nanoscale from small molecules. This method involves a physical and chemical process correlated with hydrolysis, condensation, polymerization, gelation, drying and densification, as shown in **Figure 1d [26]**. The name sol-gel originated from the fact that nanoparticles or molecules in a solution (sols) aggregate and under modified conditions joined together to create a network (gel) **[27]**. In this typical chemical reaction, the starting chemicals (precursors) such as metal salts or alkoxides are dissolved in an alcohol or aqueous solvent. The solvent molecules solvating metal cations are converted into hydroxo (OH^-) or oxo (O^{2-}) ligands, resulting to metal hydroxides. Eventually, the condensation reaction happens to fabricate M-O-M polymeric frameworks. The reaction temperature and time, pH and catalyst are the most important parameters to be controlled during the reaction **[28]**. There are lots of advantages to this synthesis method including a low cost simple route, relatively low temperature preparation method, simple equipment to be utilized, manipulation of the particle size and shape, similar compositions, high purity and low thermal treatment temperatures **[29]**. A few examples of this synthesis technique: Zhao et al. **[30]** reported highly selective NO_2 gas on p-type nanocrystalline NiO thin film sensors synthesized by sol-gel dip coating using a mixture of nickel acetate ($NiC_4H_6O_4 \cdot 4H_2O$), ammonia ($NH_3 \cdot H_2O$) and ethylene glycol monomethyl ether (C_3H_8O) as the precursors. The highly selectivity of NO_2 at the working temperature of 150 ^{o}C from the NiO thin films based gas sensors was

noticed, depicting a capability in gas sensor devices with low-energy consumption. Sta et al. **[31]** reported that lithium doped nickel oxide (NiO:Li) thin film sensors that were prepared by sol gel spin coating technique on glass substrate revealed a relatively bigger response than the pure NiO films, when assessed at various hydrogen gas concentrations in dry air conditions. Gawali et al. **[32]** showed pure NiO and Ce doped NiO nanoparticles that were highly sensitive and selective towards NO_2 gas, as illustrated in **Figure 1e**.

1.3 Hydrothermal/solvothermal synthesis

The hydrothermal method is one of the most typical synthesis techniques to prepare metal oxide, metals, and perovskite type oxides in the shape of fine particles. This synthesis method includes hydrolysis and condensation of metal salt, in the existence of water (hydrothermal) or solvent (solvothermal) at elevated temperature (~ 300 ^{o}C) and pressure (~ 10 atmosphere), to develop ultrafine MOX or metal particles, as shown in **Figure 1f [33]**. The chemical reaction is established for various hours (6 – 24 hours) resulting to nucleation and growth of nanoparticles. In addition, this method offers a relatively good control over homogeneity, chemical composition, particle and/or grain size, phase and structural morphology of the end products **[18, 34]**. The hydrothermal method could treat some nanomaterials that are difficulty synthesized with other methods **[35]**. Yu et al. **[36]** reported hierarchical net-like NiO architectures that were prepared by a simple hydrothermal procedure. The gas sensing outcomes depicted that the multiple system NiO architectures constructed by nanowires which have continuous structure (C-N NiO) demonstrated an improved gas sensing performance compared to its counterpart discontinuous net-like nanorods constructed NiO (D-N NiO) nanostructures, which is probable assigned to efficient transportation of charge carrier and abundant unlocked diffusion

7

passage by this novel nanostructure. The D-N NiO structures has a fragmented net with a large quantity of mechanical lap points, see **Figure 1g**, which behaves like obstacles, significantly prevents the effectiveness and directional transmission of charge carriers as well as mechanical nanojunctions. While in **Figure 1h**, the C-N NiO structures display a continuous hierarchical net-like nanostructure with a few nanojunctions. This special morphology enhanced the transmission efficiency of holes and therefore, the substantial improvement on gas sensing performance was noticed. Kuang et al. **[37]** depicted that the NiO hollow spheres **(Figure 1i)** with fluffy texture surface were successfully synthesized by a facile hydrothermal process and followed by calcination, were bubbles behaved as the template. NiO hollow spheres displayed an excellent sensitivity and selectivity towards 100 ppm ethanol due to hollow morphology and relatively high specific surface area. In this typical procedure, the nickel chloride and urea were used as precursors, and deionized water as a solvent. Li et al. **[38]** studied sensitive and selective to 100 ppm of formaldehyde gas sensor based on NiO nanowires at the working temperature of 200 ^{o}C. NiO nanowires were prepared by a simple hydrothermal route using nickel chloride hexahydrate ($NiCl_2 \cdot 6H_2O$), sodium oxalate ($Na_2C_2O_4$) and ethylene glycol (EG) as precursors at 220 ^{o}C for 12 hours.

1.4 Microemulsion

Microemulsions are clear and thermodynamically steady dispersions consisting of two immiscible liquids, and at least a third chemical constituent, particularly a surfactant. A transparent microemulsion is homogeneous at a macroscopic level and heterogeneous mixture at molecular and supramolecular scales **[39]**. This process of microemulsion is widely used in oil recovery, pharmaceutics, cosmetics, detergency, lubrication etc. This process is classified into water-in-oil (w/o) and oil-in-water (o/w)

microemulsions, as illustrated in **Figure 1j and k**, respectively. In w/o microemulsion, the water is homogeneously distributed in an organic media with the assistance of the surfactant, while in the o/w, the oil is distributed in water. The surfactant molecules may create a single layer at the interface between the water and oil, with the surfactant molecules consist of hydrophobic tails dispersed in the oil phase and the hydrophilic head groups in the aqueous phase. In addition to these two classifications of microemulsions, the water-in-supercritical-CO_2 (w/sc-CO_2) microemulsion has been discovered to be one of the emerging classes of microemulsion **[40]**. In w/sc-CO_2 microemulsion, the water droplets are distributed in supercritical carbon dioxide. The addition of surfactant (ionic or non-ionic) and/or co-surfactants and below some critical concentration leads to stability in the system. The formation of "micelles" or "inverse micelles" is relying upon the concentration of water and organic liquid. Micelles are created with surplus water, while inverse micelles are generated in the surplus of organic liquid or oil. The micelles or inverse micelles collide leading to the creation of various configurations and the possibility of creating nanomaterials of various structures. This is one of the promising methods for producing nanoparticles due to simplicity, economically friendly, long term stability and enhanced bioavailability, high solubilisation capacity for hydrophilic and lipophilic drugs **[41 - 43]**. Recently, most of the studies have been done on this synthesis method; Du et al. **[44]** revealed that the precursors used during the microemulsion synthesis were nickel chloride, ammonia and deionized water, the surfactant and cosurfactant of triton X-100 and cyclohexane, respectively. The particle size of NiO was varied in the range of 11.5 to 31.5 nm by altering the ratio of water, surfactant and oil in the microemulsion, mixing procedure and calcining temperature. Therefore, highly sensitivity and selectivity towards hydrogen sulfide,

ethanol and nitrogen dioxide were noticed from NiO based gas sensors. Wang et al. **[45]** showed that the NiO nanospheres were distributed in ethanol containing SDS and sonicated to create homogeneous suspension, and then a significant content of silver nitrate (AgNO₃) aqueous solution was incorporated to this suspension above, generating a microemulsion. Ganguli et al. **[40]** reviewed microemulsion –based synthesis of nanocrystalline materials. **Figure 1l** presents the creation of nanorods of nickel oxalate prepared using cationic surfactants cetyltrimethylammonium bromide (CTAB). This observation is a sign that cationic surfactants result to anisotropy and that nanorods of some divalent metal carboxylates could be accomplished.
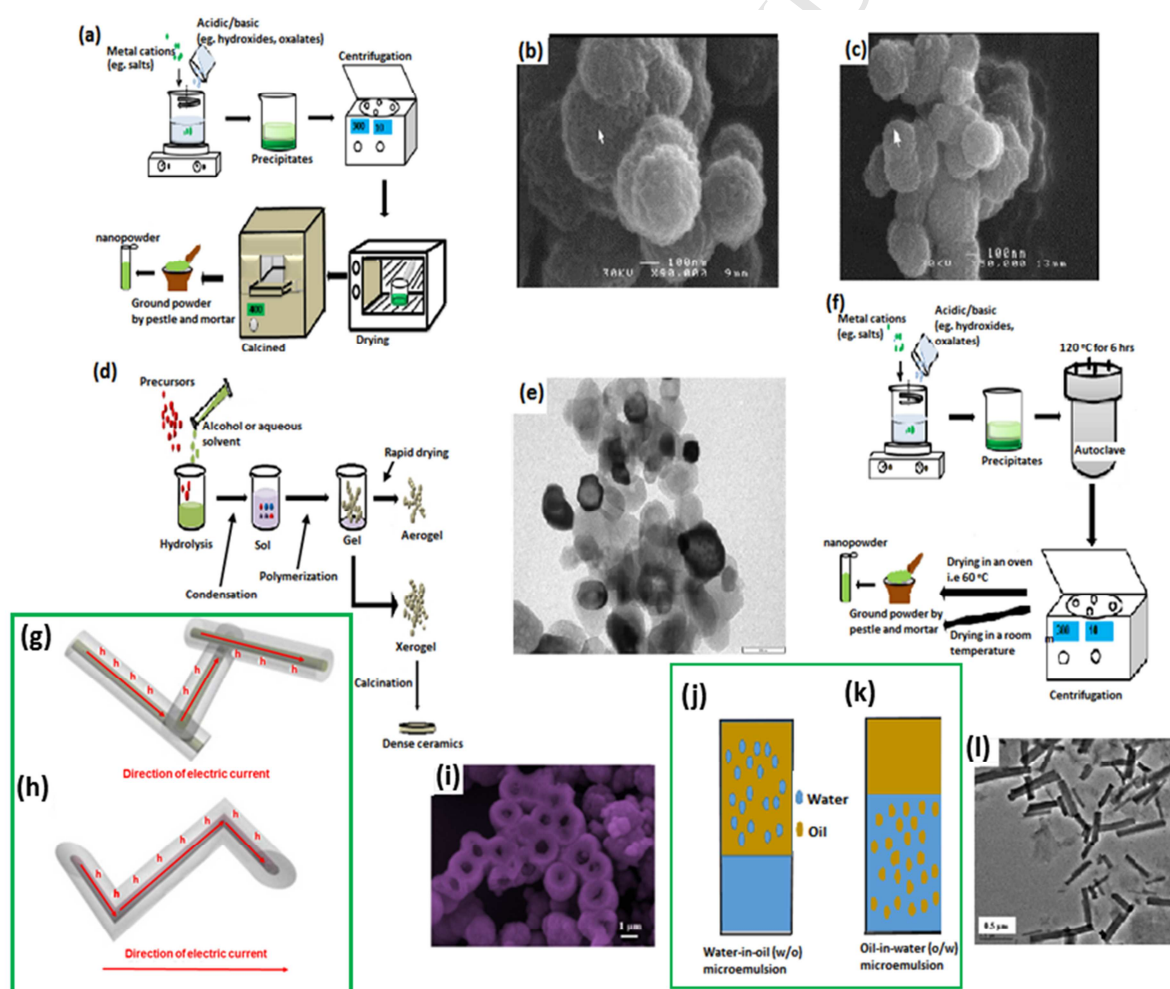

Figure 1: (a) Schematic illustration of chemical/co-precipitation method. SEM micrographs of (b) as-synthesized Ni(OH)$_2$ and (c) NiO calcined at 350 ^{o}C. (Reprinted with permission from

Ref.**[20]**. Copyright 2004: Elsevier). (d) Schematic diagram of sol-gel synthesis. (e) TEM images of Ce doped NiO. (Reprinted with permission from Ref. **[32]**. Copyright 2018: Elsevier). (f) Sketch of hydrothermal method. (g) D-N NiO, (h) C-N NiO. (Reprinted with permission from Ref. **[36]**. Copyright 2017: Elsevier). (i) SEM micrographs of NiO hollow spheres. (Reprinted with permission from Ref. **[37]**. Copyright 2018: Elsevier). Schematic illustration of (j) water-in-oil (w/o) and (k) oil-in-water (o/w) microemulsion. (l) TEM images for nickel oxalate dehydrate prepared using CTAB/1-butanol/n-hexane. (Reprinted with permission from Ref.**[40]**. Copyright 20110: Royal Society of Chemistry).

Studies have revealed that NiO has drawn a great interest in gas sensing applications due to its tremendous properties **[46 - 49]**. However, there is still a gap with regards to the NiO based gas sensors synthesized by this microemulsion method. In actual fact, the p-type NiO sensing performance has relatively low sensitivity compared with some of the n-type SMO. Nonetheless, NiO has been discovered to have excellent catalytic action through the oxidation of volatile organic compounds. In this regard, the improvement on gas sensing characteristics of NiO is a necessity. Therefore, doping of NiO with various dopants and construction of heterostructures with other n-type SMO, have found to results in the enhancement of gas sensing characteristics, refer to **Figure 2a**. Hence, the number of publications on doped NiO and heterostructures increased drastically since the year 2010. There are different synthesis techniques that can be used to prepare NiO sensors. However, in this work we focussed on discussing chemical and/or co-precipitation, sol-gel, hydrothermal/solvothermal and micro-emulsion methods due to the unique properties that they offer. **Figure 2b** verified that the hydrothermal technique is considered to be the relevant method for preparation of NiO gas sensors. This is due to the dominance over the homogeneity, particle size and morphology of the final products. **Table 1** shows a comparison study on the gas sensing characteristics of NiO nanostructures synthesized by different methods.

Table 1: A literature survey on NiO gas sensing properties synthesis by various methods.

Materials	Synthesis procedure	Gas	Conc. (ppm)	T_{op} (^{o}C)	Response	Refs.
NiO nanosheets	Hydrothermal	Ethanol	50	250	65	[50]
NiO	Hydrothermal	Acetone	100	260	13.51	[9]
NiO flake-flower	Hydrothermal	Ethanol	400	300	32	[51]
NiO nanoflower	Hydrothermal	Ethanol	200	300	40	[52]
NiO	Co-precipitation	Benzaldehyde	100	300	250	[23]
NiO-SnO$_2$ nanoflower	Co-precipitation	Ethanol	20	320	94.8	[24]
NiO-RuO$_2$	Co-precipitation	Ethanol	1000	350	29.1	[25]
NiO-SnO$_2$	Co-precipitation	Formaldehyde	100	200	27.6	[53]
NiO:Ce nanoparticles	Sol-gel	NO$_2$	40	150	29	[32]
NiO thin films	Sol-gel	H$_2$	3000	175	65	[54]
NiO thin films	Sol-gel	NO$_2$	20	150	2.6	[30]
NiO	Micro-emulsion	H$_2$S	100	150	9.0	[43]
		Ethanol	100	200	3.0	
		NO$_2$	100	150	2.7	
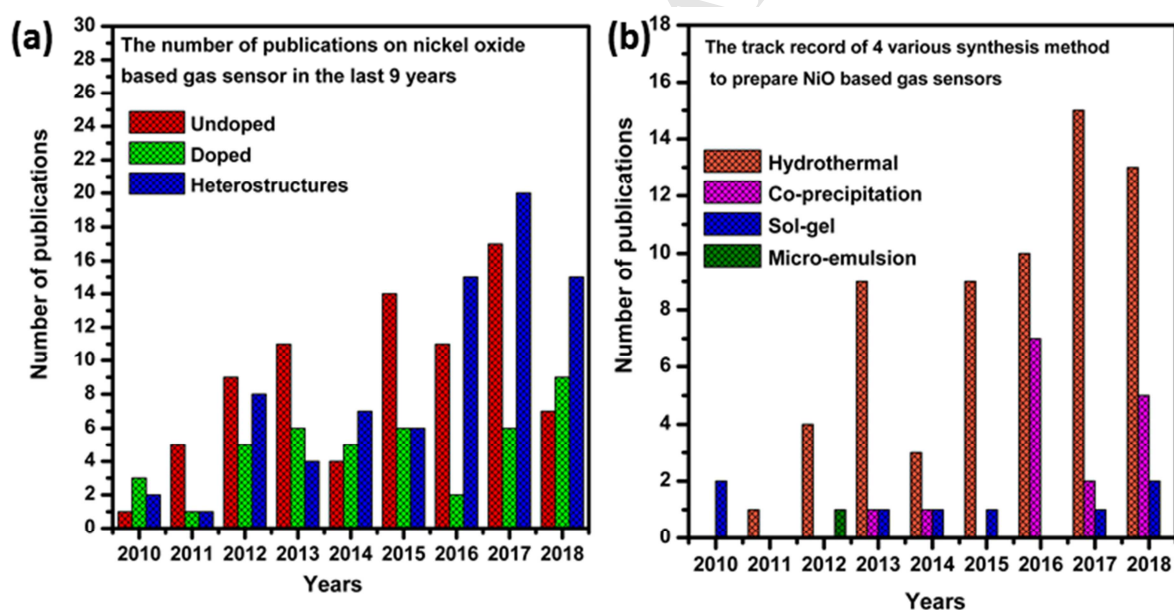
Figure 2: (a) The number of publications on NiO based gas sensor over the period of 9 years, since from 2010 up to date. (b) The track records of 4 various synthesis techniques used to prepare NiO based gas sensors.

2. Gas sensing mechanism of NiO

In principle, the gas sensing properties of SMO emerge from the alteration of charge carrier concentration due to the reaction between the target gas and the

surface of SMO. To add on that, this gas sensing characteristics of SMO is governed by the oxidation-reduction reactions of the chemisorbed oxygen with the detected gases occurring on the surface. The charge carrier concentration of SMO in atmospheric air is a primary factor for governing the gas response **[55, 56]**. In a chemoresistive-type sensors, a SMO is drop-casted across two or more electrodes (platinum (Pt) electrodes) which quantify the variation in the behaviour of electrical resistance of the SMO in the existence of the target gas, as shown in **Figure 3a [57, 58]**. When a p-type NiO with holes as a majority of carrier, is exposed to clean air (~ 21 % oxygen gas), electrons are extracted from the NiO and attracted to the oxygen species, which is chemisorbed on the surface of the sensing material. This creates more holes, which result to an increase in electrical conductivity, therefore forming the depletion layer **Figure 3b and c**. This decreases the potential barrier height situated at the grain boundary with more electron flow, resulting in a relatively high sensor current flow (low sensor resistance) in relatively clean air ambient **[59, 60]**. The involved reaction in the SMO surface and with the adsorbed oxygen species can be noticed in the following manner:

$$O_{2(gas)} + e^- \rightarrow O_{2(adsorbed)}^- \qquad (\text{T}_{op} < 100\ ^oC) \qquad (1)$$

$$O_{2(gas)} + 2e^- \rightarrow 2O_{(adsorbed)}^- \qquad (100\ ^oC < \text{T}_{op} < 300\ ^oC) \qquad (2)$$

$$O_{2(adsorbed)}^- + e^- \rightarrow O_{2(adsorbed)}^- \qquad (\text{T}_{op} > 300\ ^oC) \qquad (3)$$

Generally, the adsorbed oxygen is greatly dependent on operating temperature (T_{op}): having O_2^- nature less than 100 ^oC, O^- in the range of 100 to 300 ^oC, and O^{2-} greater than 300 ^oC **[60, 61]**. When a p-type NiO SMO is introduced to a reducing gas such as CO, H_2S, ethanol and NH_3, the molecules are adsorbed on the surface
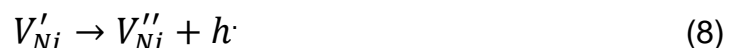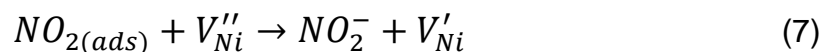
13

and they interact with the chemisorbed oxygen ions and donate electrons into the MOX. The amount of holes will decrease and the depletion layer becomes thicker (high electrical resistance), therefore, electrical conductivity decreases, as illustrated in **Figure 3d**. This behaviour of an expansion in the depletion layer, leads to the growth in the potential barrier height located at the boundary site. In the case of oxidising gases including CO_2, O_2 and NO_2, the analyte gas interacts with the chemisorbed oxygen ions on the surface and extracts electrons from the metal oxide. The concentration of holes increases and the depletion layer becomes thinner (low electrical resistance) and therefore, electrical conductivity increases, as shown in **Figure 3e [63, 64]**. In the case of n-type SMO such as ZnO, TiO_2 and SnO_2 the opposite occurs, when exposed to reducing gas the electrical resistance decreases. When exposed to oxidising gas electrical resistance escalates. We will briefly discuss the n-type sensing mechanism on the later sections, because of the p-n heterostructures constructed between p-type NiO and other n-type SMO. The resistance of the SMO may elevate or decline on exposure to the gas relying on the majority charge carrier and nature of gas reacting with the surface. Anyway, according to the defects chemistry of NiO, Unutulmazsoy et al. **[65]** unpacked that nickel vacancies and electron holes (h·) are the most predominant defects in NiO structures. However, the ionization degree of nickel vacancies: singly negatively charged nickel vacancy (V'_{Ni}) and doubly negatively charged nickel vacancy (V''_{Ni}) using the Kröger-Vink notation, still not clear. These V'_{Ni} and V''_{Ni} exist simultaneously in NiO structures, the proportion of single and doubly ionized vacancies is dependent on the temperature. The V'_{Ni} is predominant at low temperatures, while V''_{Ni} is predominant at high temperatures (900 – 1200 ^{o}C). The chemical reaction for addition of oxygen from the gas phase into the lattice is:

14

$$\frac{1}{2}O_2 \leftrightarrow O_O^\times + V_{Ni}'' + 2h^\cdot \tag{4}$$

whereby $O_O^\times$ represents oxygen ion on oxygen atom and the nickel vacancies can alter valence according to:

$$V_{Ni}'' + h^\cdot \leftrightarrow V_{Ni}' \tag{5}$$

A few examples are given on how these different gases behave as they interact with SMO, in particularly gases such as NO_2, H_2S, and NH_3 for the purpose of indoor air quality and food quality monitoring. The room-temperature NO_2 gas sensing mechanism established on the NiO was described upon exposure to NO_2 gas by Zhang et al. **[66]**, initially NO_2 gas molecules physically adsorb onto the surface of NiO sensor (see reaction 6). The physisorbed NO_2 gas molecules withdraw the electrons from nickel vacancies and result to a singly negatively charged state V_{Ni}', which can spontaneously go back to V_{Ni}'' , abandon $h^\cdot$ in the valence band NiO at room temperature, refer to reaction (7) – (8). During this process, the hole concentration of the NiO enhances, leading to the improvement in the electrical conductivity of the NiO sensor **[67]**. The similar observation is also noticed by Oosthuizen et al. **[68]**.

$$NO_{2(gas)} \rightarrow NO_{2(ads)} \tag{6}$$

$$NO_{2(ads)} + V_{Ni}'' \rightarrow NO_2^- + V_{Ni}' \tag{7}$$

$$V_{Ni}' \rightarrow V_{Ni}'' + h^\cdot \tag{8}$$

In the case of reducing gas, when NH_3 gas interacts and/or adsorbed on the surface, it interacts with oxygen species and donates electron back to the NiO surface according to the following reaction;

$$\frac{2}{3}NH_3 + O_O^\times \leftrightarrow H_2O + \frac{1}{3}N_2 + 2e' + V_{\ddot{O}} \tag{9}$$
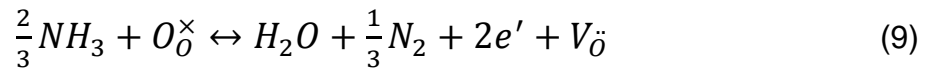
The $V_{\ddot{O}}$ and e' denotes oxygen vacancy with double positive charge and negatively charged electron, respectively according to Kröger-Vink defects notation. The movement of electrons back to the surface of NiO makes it less p-type SMO. This means the hole concentration is decreasing, resulting to the increase in surface resistance **[69, 70]**. When the H_2S reducing gas is exposed to the sensor, the surface chemical reaction can be represented as:

$$H_2S + 3O_O^\times \leftrightarrow SO_2 + H_2O + 3V_O^\times \tag{10}$$

$$V_O^\times \leftrightarrow V_{\dot{O}} + e' \tag{11}$$
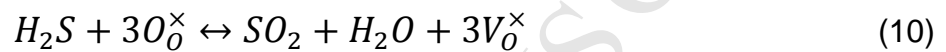
In this case, when H_2S gas molecules interact with adsorbed oxygen species and donate the trapped electrons back to the conduction band, therefore the electrical conductance of NiO decreases **[71]**.
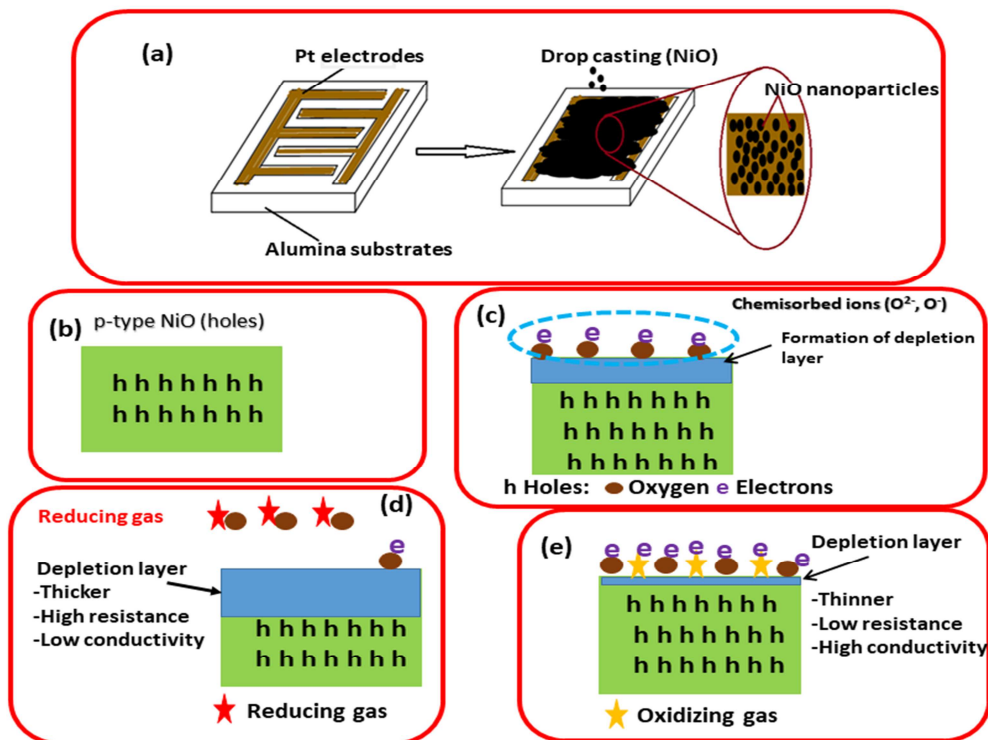
Figure 3: (a) Schematic illustration of Pt-electrode on nickel oxide. (b) p-type NiO based gas sensors. (c) The p-type NiO during the exposure of oxygen. (d) The decrease in a potential barrier height on NiO nanostructures. (e) The NiO nanostructure sensor upon the exposure of reducing gas. (f) The increase in a potential barrier height on NiO nanostructure sensor. (g) The NiO based gas sensor upon the exposure of an oxidizing gas.

To the best of our knowledge it is very popular that the operating temperature has a serious influence on the gas sensing characteristics. There are various features including oxygen species, rates of adsorption and desorption, the charge – carrier content and the Debye length, rely much on the sensor working temperature. The Debye length (λ_D) **[72 - 75]** for a SMO can be estimated as follows:

$$\lambda_D = \sqrt{\varepsilon k T \big/ q^2 n_c} \tag{13}$$

Where, λ_D is dependent to dielectric constant (ε), Boltzmann's constant (k), elementary charge (q = 1.6 × 10^{-19} C), absolute temperature (T) and the carrier charge concentration (n_c) of SMO. By contrast, the MOX based gas sensors become highly sensitive when relatively large quantities of active electrons engage in the reaction at the optimum temperature. Amongst the various factors influencing the gas sensing performance, the grain size (d_m) is considered as a vital parameter. The sensing resistance in air (R_a) and in the analyte gas (R_g) varies as the d_m changes. Similar work was conducted by Mirzaei et al. **[76]**. As depicted **Figure 4a** for SnO$_2$, a rise in d_m from 4 to 6 nm induces a considerable decrease in the resistances, whereas an additional increase in d_m leads to a gradually increase in both resistances. The alteration at a critical grain size (d_m = 6 nm) is assigned to the development of an electron-depletion layer on the surface of the particle. Because the λ_D is kept steady for a particular material at a precise temperature and carrier

concentration, the proportion of λ_D is modified by the change in d_m. In the case of d_m < $2\lambda_D$, the entire particle experiences electron-depletion, while depletion is witnessed merely at the surface region. In the later stage, the grain boundary potential (double Schottky barrier) for electron movement is not dependent on the d_m. Therefore, the sensor resistance is not dependent on the d_m. Though, in the other case of d_m < $2\lambda_D$ the resistance is greatly dependent on d_m. Thus, the gas sensing response (R_a/R_g) also depends on the d_m. The gas response drastically decreases with an increase in d_m up to ~ 10 nm and then becomes virtually independent d_m > 15 nm, as illustrated in **Figure 4b**. In conclusive remarks, these results depicted that by controlling the d_m to be less than $2\lambda_D$ is very crucial in order to prepare a MOX based gas sensor with a high sensitivity or good sensing properties **[77]**.
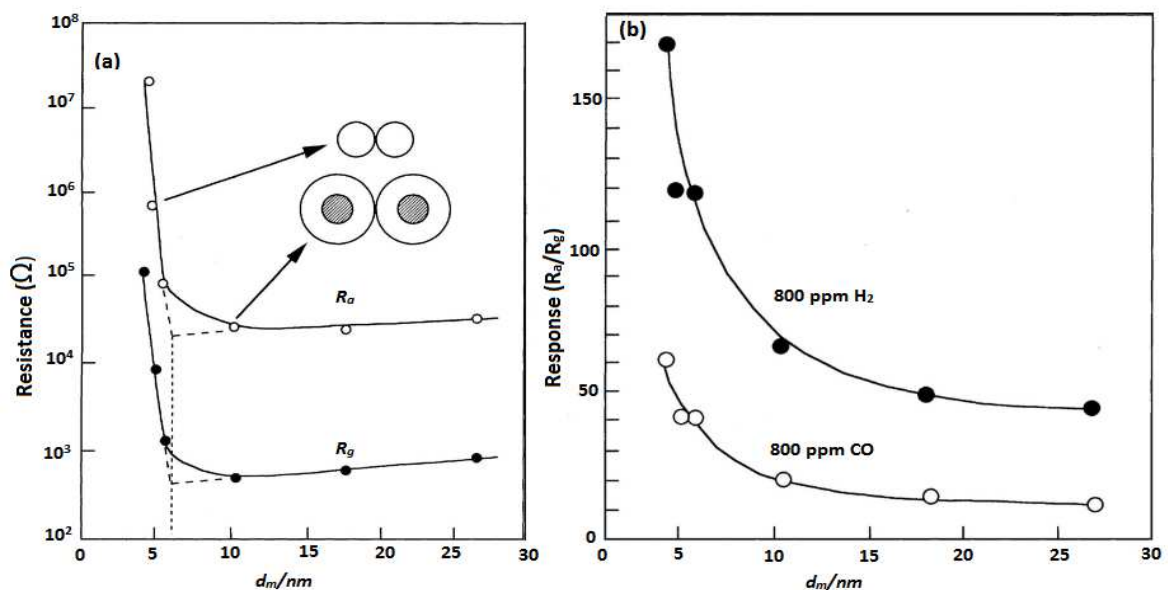
Figure 4: (a) Effect of grain size of the SnO_2 on sensing resistance in dry air (R_a) and in 800 ppm H_2 (R_g) at operating temperature of 300 ^{o}C. (b) SnO_2 grain size influence on gas sensor response towards 800 ppm of H_2 and CO in air at working temperature of 300 ^{o}C. (Reprinted with permission from Ref. **[76]**. Copyright 2018: Elsevier).

Furthermore, it was revealed that p-type MOX such as NiO and CuO have numerous related properties. Consequently, the shells developed from these

18

nanostructured materials ought to have same characteristics. A typical example, Xu et al. **[78]** studied the TEA sensors-based on α-Fe$_2$O$_3$-NiO and α-Fe$_2$O$_3$-CuO core-shell nanorods (C-S NRs) heterostructures. Porous α-Fe$_2$O$_3$ nanorods were prepared via hydrothermal process using alumina substrates, as depicted in **Figure 5a.** The p-type shell was prepared using a pulse laser deposition (PLD) method. The thickness of a shell was maintained through varying the applied laser pulse. The response of α-Fe$_2$O$_3$-NiO and α-Fe$_2$O$_3$-CuO sensors enhanced rapidly by increasing the thickness of the shell to 13 and 12.4 nm, respectively. After the thickness of the NiO/CuO shell p-type was more than the optimum value, the layer of the shell did not permit any exposure of α-Fe$_2$O$_3$ NRs to the target gas. Therefore, its holes couldn't be depleted completely and participate in the gas reaction. The maximum response of the C-S NRs heterostructure was noticed for the p-type shell with a thickness layer that is very close to λ_D (NiO or CuO). **Figure 5b – d** displays the holes in a p-type shell that is thinner compared to λ_D, which will be depleted completely when exposed to air, resulting to a relatively higher resistance. When the thickness of the shell expanded to the size of the λ_D, the depletion layer was considered as λ_D ((NiO or CuO) + λ_D (α-Fe$_2$O$_3$)). In this regard, the R_a achieved the relatively highest value and as a result the superior response was noticed. With regard to the p-type shells being thicker than λ_D, the holes in the shell were moderately depleted by due to the construction of the p-n heterojunction. Furthermore, the level of the shell was incomplete hole-accumulation. As a result, the thicker shell had a relatively less effect on the resistance modulation, causing a low gas response.
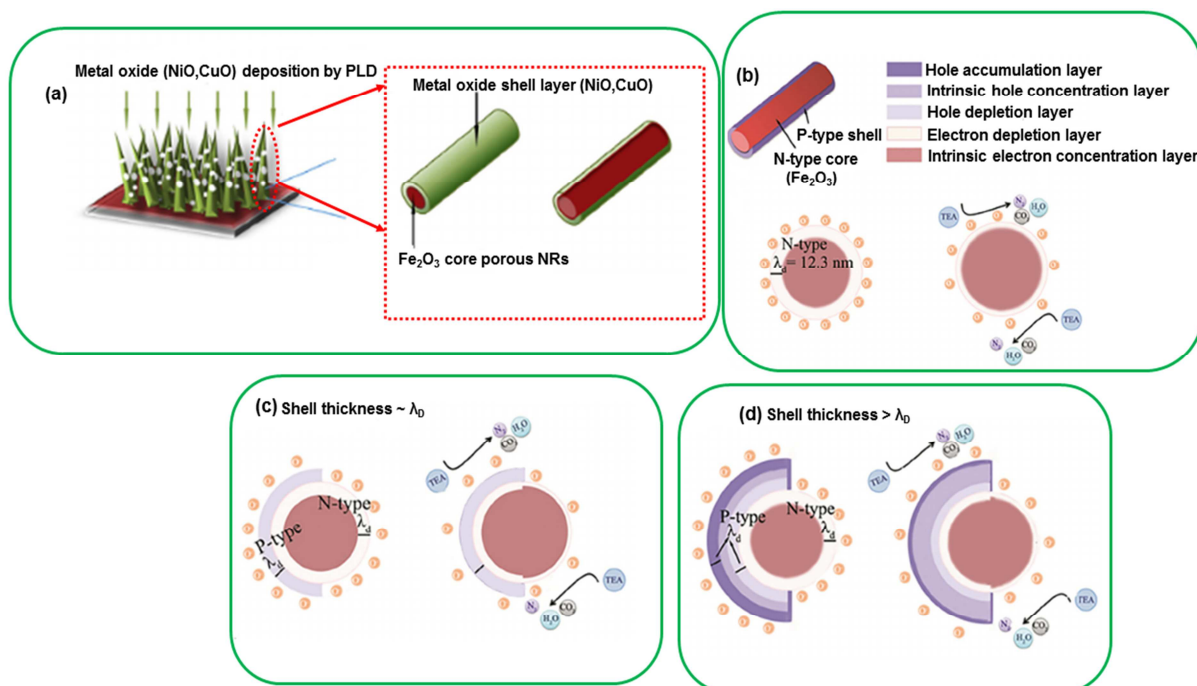
Figure 5: (a) α-Fe$_2$O$_3$@NiO/CuO core-shell nanorods (C-R NRs). Schematic illustration of mechanism for TEA gas sensing: (b) pure α-Fe$_2$O$_3$ NRs; (c) Core-shell heterostructure containing a p-type shell thickness ~ λ_D. (d) Core-shell heterostructure containing a p-type shell thickness > λ_D. (Reprinted with permission from Ref. **[78]**. Copyright 2017: Elsevier).

In a nutshell, the sensitivity of the sensor can be enhanced drastically by altering the features of nanostructure such as grain size. In the occasion of big grain where grain size (d_m) >> thickness of the space charge layer ($2\lambda_D$), the conductance is restricted by Schottky barrier at grain boundaries, as shown in **Figure 6a**. If d_m = $2\lambda_D$, conductance is restricted by necks between the grain, while in the case of d_m < $2\lambda_D$ conductance is highly affected by every grains, as depicted in **Figure 6b and c**. The porous metal oxides with a relatively large surface area have been earmarked to be relevant sensing materials that increase the gas sensitivity. The sensitivity of MOX gas sensors can be intensified by introducing the dopants such as noble metals, rare earth oxides, transition metals and other n-type metal oxides **[79]**.
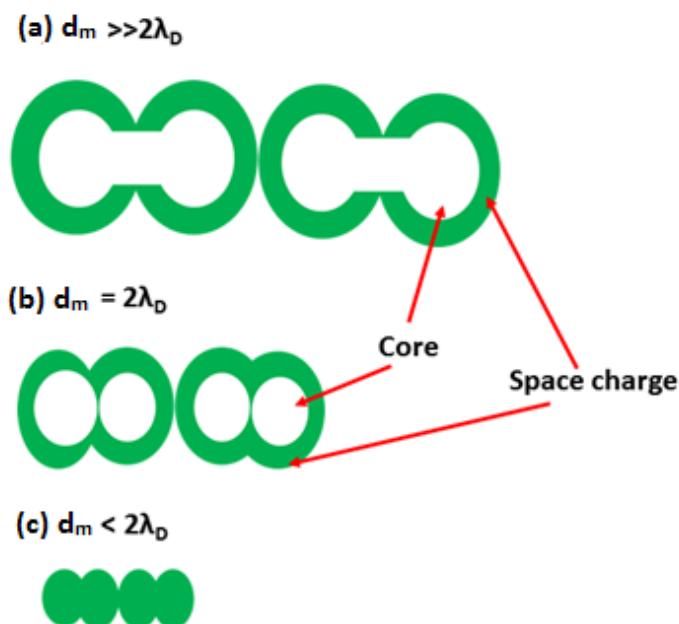
Figure 6: Three mechanisms of conductance in MOX gas sensors. (a) $d_m \gg 2\lambda_D$, grain boundary control, (b) $d_m = 2\lambda_D$, neck control, and (c) $d_m < 2\lambda_D$, grain control**.** (Reprinted with permission from Ref. **[79]**. Copyright 2018: Elsevier).

3. Effect of noble metals on the NiO gas sensing properties.

The noble metals such as palladium (Pd), platinum (Pt), gold (Au) and silver (Ag), are very famous as active catalysts, and have been identified to be very influential on many SMO gas sensors. The incorporation of noble metals to the SMO based gas sensors is very constructive way of manipulating and improving the gas sensing characteristics **[80 - 82]**. For example, Rai et al. **[83]** investigated the role of Pd nanoparticles in gas sensing behaviour of Pd@In$_2$O$_3$ yolk-shell nanoreactors. The incorporation of In$_2$O$_3$ with Pd nanoparticles enhanced the response for reducing gases, but lowered the response for oxidizing gases. Zhang et al. **[84]** prepared Au-decorated SnO$_2$ porous hollow spheres for chemical sensor applications. These results depicted that apart from the porous structure, the catalytic effect of Au nanoparticles played a role in improving gas sensing properties. Penza et al. **[85]**

reported that NO$_x$ gas sensing properties of WO$_3$ sensor were activated by incorporation of noble metals such as Pd, Pt and, Au layers.

Herein, we review the influence of these noble metals on the NiO gas sensing properties. This influence has formally been categorized as chemical or electronic according to two basic sensitisation mechanisms. Firstly, in the chemical mechanism, the SMO itself behaves as a chemical catalyst. The additives character is to enhance the rate of reaction of the gas molecules, which are firstly adsorbed on the noble metal and then moved to the SMO surface in a so-called spill-over phenomenon [86]. In simple terms, this phenomenon involves the enhance in the amount of oxygen species and accelerates the surface reaction, inducing the increase in hole accumulation layer (HAL), as illustrated in **Figure 7a and b.** This oxygen species extract more electrons which lead to the creation of more holes and therefore, the resistance was reduced. Secondly, in the electronic sensitization, Fermi level of noble metals is relatively lower than that of SMO based gas sensors. In this regard, charge carriers are relocated, while the electrons are transported from the SMO into the noble metal until the Fermi level of two nanomaterials reach equilibrium. During this mechanism, the noble metals and SMO become negatively and positively charged, respectively. The energy bands in SMO are curved and Schottky barrier is created at the interface. The Schottky barrier can resist the recombination of separated electron-hole pairs and enhance the response to the analyte gas. Another scenario is that the noble metal atoms incorporated into the SMO will substitutes some metal atoms. This will change the crystallographic features such as bond length and lattice parameter of the material i.e. lattice distortion. Due to that the negative and positive charge centres of the octahedron will be rearranged and create dipole moments inside. Then a local electric field will be

created in the entire crystal, promoting the electron-hole pair separation **[87]**. In practical terms, electrons from conduction band of SMO are transported into noble metals, due to dissimilarities in work function generating Schottky barriers at the interface between noble metals and SMO. Consequently, additional HAL near SMO surface is formed, as illustrated in **Figure 7c**. This behaviour is also increases the HAL due to more holes that were formed during the extraction of electrons.

These mechanisms were noticed previous by Wang et al. **[88].** The Au-loaded NiO based sensors revealed the enhanced sensing properties in terms of relatively good sensitivity, low detection limit, relatively better selectivity, quick response and acceptable reproducibility compared with its counterpart pure NiO sensor. Tong et al. **[89]** revealed NiO nanosheets mesoporous that were prepared by a surfactant-less hydrothermal synthesis followed by thermal oxidation, whereas the Pd nanoparticles were decorated by in-situ reduction of palladium complex, as shown in **Figure 7d**. **Figure 7e and f** presents the SEM micrographs of the fabricated sensor microchips and Pd-NiO nanosheets, respectively. The analysis of gas-sensing exhibited that this sensor is more effective on detecting hydrogen at low concentration (25 - 500 ppm) with fast response – recovery times (91 – 52 s), relatively high sensitivity (23 - 224 %) and stability, as illustrated in **Figure 7g.** Fu et al. **[90]** revealed that the composite of Pt-NiO gas sensors is more selective to the ethanol vapour than the pure NiO. Additionally, this Pt-NiO sensor with nanotube morphology showed a response value of 20.85 towards 100 ppm ethanol vapour at working temperature of 200 ^{o}C, as shown in Figure **7h and i**. This improved sensing behaviour is assigned to the effect of Pt on the chemical sensitization of the analyte gases and the electronic sensitization **(see Figure 7j)** of NiO. In air, each Pt nanoparticle composed of Pt and Pt^{4+} creates a redox reaction Pt^{4+}/Pt^{0}. To obtain electronic equilibrium with the Pt

23

nanoparticles, the Fermi level of NiO will be moved and pinned at the Pt^{4+}/Pt^0 electrode potential, which forms hole-accumulation layer. This implies that holes concentration will be enhanced, while the resistance reduces. Then, in the presence of a reducing gas, the target gas donate electrons, this means hole accumulation layer decreases and resistance increases.
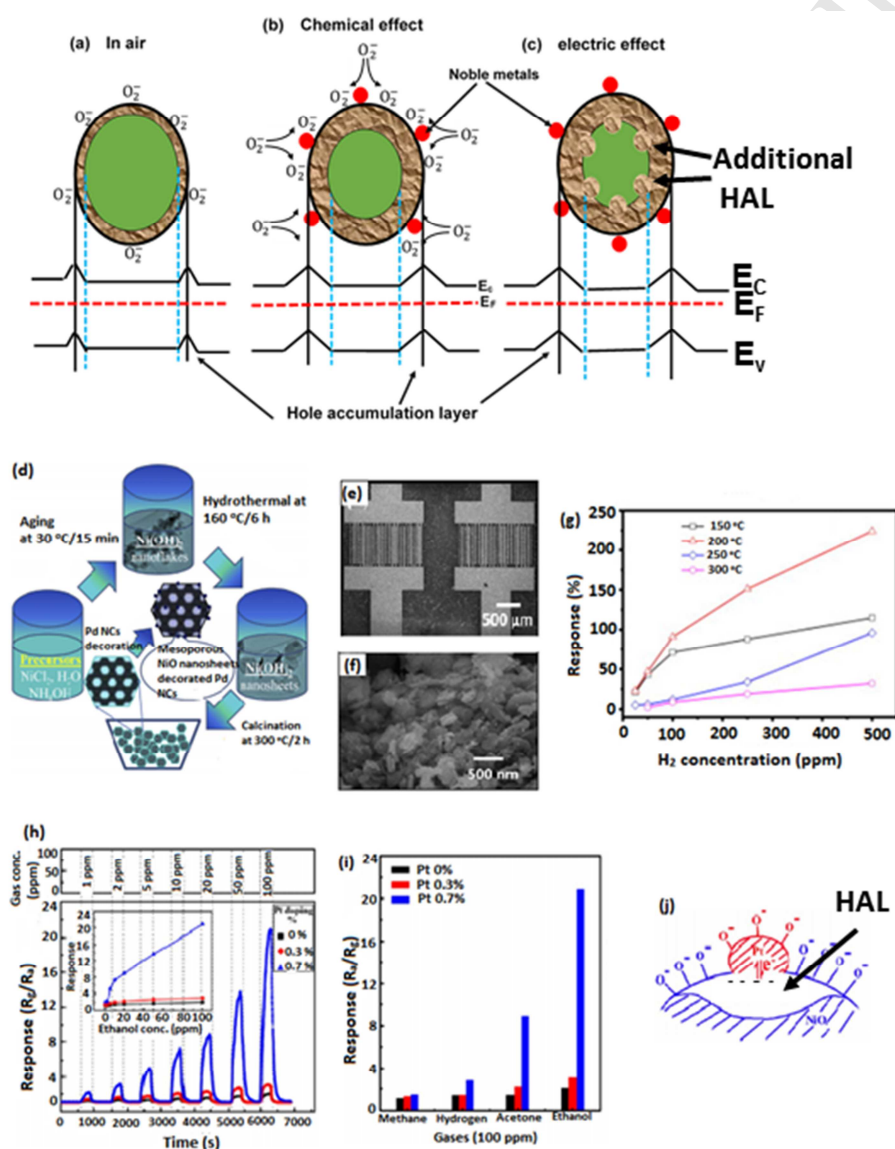
Figure 7: (a) Schematic diagram presenting the depletion layer of an unsensitised NiO nanostructured material. Schematic illustration of (b) chemical and (c) electronic sensitization of a noble metal incorporated into NiO. (d) Preparation process of the NiO nanosheets consist of mesoporous decorated with Pd nanoparticles. SEM micrographs of the fabricated (e) sensor microchips, and (f) Pd-NiO nanosheets. (g) The response

against the concentration of H_2 gas on various working temperature. (Reprinted with permission from Ref. **[89]**. Copyright 2013: Elsevier). (h) Response and recovery curve of the pure NiO and NiO-Pt gas sensors towards the ethanol in the range 1 – 200 ^{o}C; the inset presents the response as function of the ethanol gas concentration for the three various gas sensors. (i) The response selectivity of the three gas detectors for the various target gases (methane, hydrogen, acetone and ethanol). (j) Schematic diagram of the electronic sensitization between NiO and Pt. (Reprinted with permission from Ref. **[90]**. Copyright 2013: American Chemical Society).

4.   Effect of transition metals on the NiO gas sensing performance.

Transitional metals (TMs) such iron (Fe), copper (Cu), nickel (Ni) and cobalt (Co) are the most widely used surface modifiers, and has been known to enhance the performance of gas sensing features. These TMs are usually decorated or deposited on the surface of MOX and they behave as surface sites for adsorbates, catalyst or promoters for surface reaction and as elements facilitating the enhancement in the thermodynamically stability of the nanostructured materials. The catalyst is known to speed-up the chemical reaction without itself undergoing, this implies that it does not alter the free energy of the reaction but minimizes the activation energy. During the synthesis of MOX decorated with TMs gas sensors, it is advisable to use the concentration within the range of 3 – 7 % as further incorporations result to improving electronic and reducing ionic conductivities **[91]**. In this section the effect of TMs decorated on NiO nanostructured materials will be discussed. However, most of the studies revealed that Fe-decorated on NiO based gas sensors is a widely used due to tremendous properties, compared to other TMs. This is because the studies based on TMs decorated on NiO are very limited, refer to **Table 2**. A typical example, Tho et al. **[92]** reported high temperature calcination for analysing influence of 3d TMs on gas sensing performance of mixed potential sensor Pt/yttria-stabilized zirconia (YSZ)/LaMO$_3$ (M = Mn, Fe, Co, Ni). The higher sensitivity

25

and selectivity behaviour towards the NO$_2$ gas were observed from the Pt/YSZ/LaFeO$_3$. However, the sensors Pt/YSZ/LaMO$_3$ (M = Mn, Co, Ni) demonstrated the poor selectivity towards NO$_2$ gas. This enhanced sensing performance was related to the elevated temperature sintering method that changed the interface of YSZ/LaFeO$_3$. On the other study, Yoon et al. **[93]** reported the gas sensing features of pure NiO and 0.18 – 13.2 at% Fe-doped NiO nanofibers synthesized by electrospinning. The response towards 100 ppm ethanol gas was improved to the maximum of 217.86 times by incorporating 3.04 at% Fe into NiO nanofibers. The improved gas sensing performance of Fe-doped NiO sensors was related to the electronic sensitization, that is, the improvement in the chemoresistive alteration due to the reduce in hole concentration caused by Fe doping. Li et al. **[94]** revealed that Fe-doped NiO sensor possess relatively best sensing characteristics even at relatively low temperature (200 – 280 ^{o}C). Amongst all the gas sensors 3.0 at% Fe-doped in NiO displayed the best response towards the 12 – 100 ppm ethanol gas at 280 ^{o}C, and extremely rapid response and recovery times of 1.0 and 3.6 s, respectively. Sun et al. **[95]** showed TEM and SEM micrographs of NiO with long and short-range mesoporous ordered in periodic behaviour, as depicted in **Figure 8a - d**. The gas sensing characteristics exhibited that the sensors consist of long-range mesoporous arranged in a periodic manner displays a relatively good ethanol sensing property than its counterpart, NiO with short-range mesoporous arranged in periodic behaviour **Figure 8e – i**. The decoration of Co and Fe on the NiO nanostructure was utilized to modify the sensing characteristics of the arranged mesoporous NiO gas sensor. However, by incorporating Fe in the optimized NiO mesoporous, the gas sensing performance was clearly enhanced. This improvement of gas sensing performance is assigned to the mesoporous nanostructure and

26

chemical state of the surface modified by the incorporation of Fe, relatively high gas adsorption, diffusion, and rate of reaction were accomplished and consequently improved gas sensing efficiency. Generally speaking, this improvement could be related by relatively big specific surface area associated with ample active sites, suitable pore size distribution for sufficient gas diffusion, and significant particle and/or grain size for efficient charge accumulation of NiO with long-range mesoporous arranged in periodic fashion. In addition, the enhancement in gas sensing features also relies in the electronic structure of TMs. These TMs have incompletely filled d-shells which enable multiple oxidation state, for example, $M^{n+}/M^{(n+1)}$ (Ni^{2+}/Ni^{3+}, Cu^{+}/Cu^{2+}). In this regard, the gas sensing molecules can easily react with this pair of different charges and undergo reactions. In terms of catalytic behaviour of TMs, detailed understanding is required on the fundamental of gas sensing mechanism **[218]**.
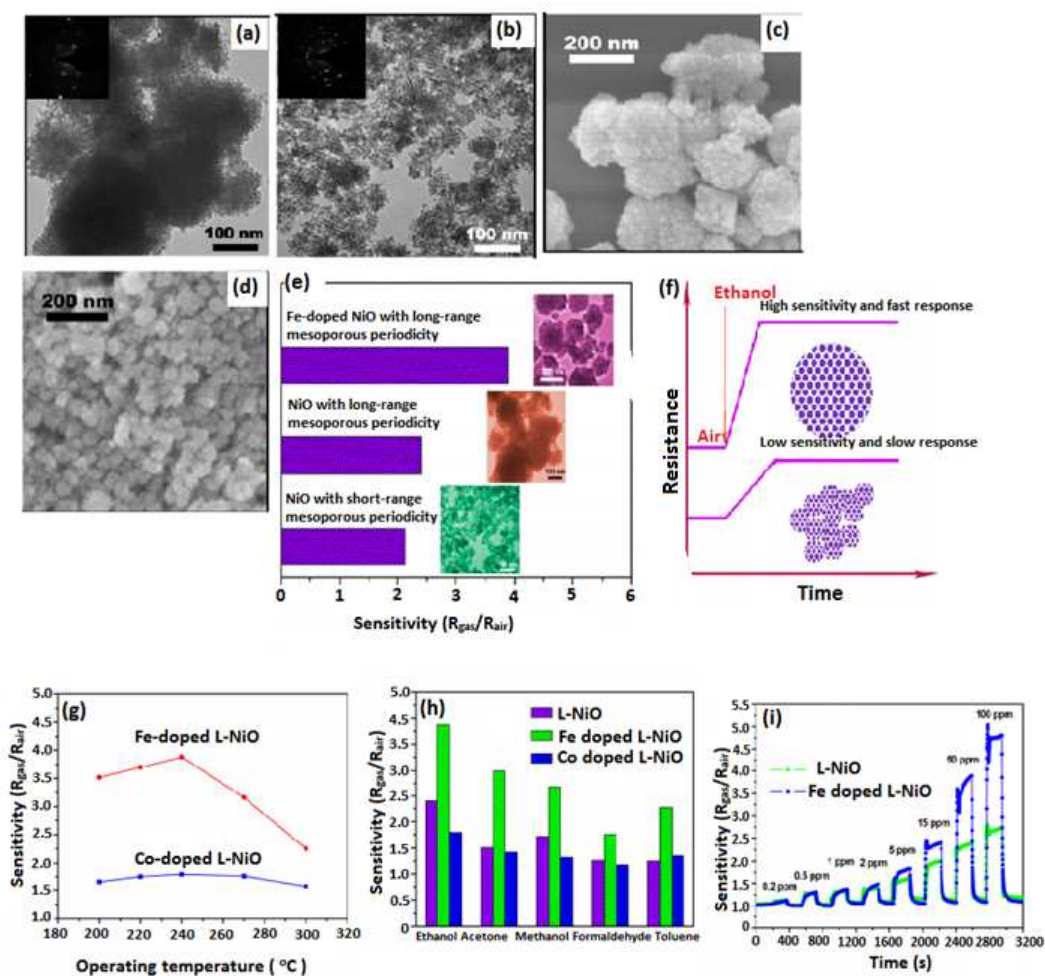
Figure 8: TEM micrographs of NiO with (a) long and (b) short-range mesoporous arranged in periodic manner. SEM micrographs of NiO with (c) long and (d) short-range ordered mesoporous periodicity. (e) The sensitivity of pure NiO and Fe-doped NiO sensors. (f) Schematic diagram of sensing factors of long-range mesoporous (L)-NiO and short-range mesoporous (S)-NiO samples. (g) Sensitivity as a function of working temperature for Fe-decorated L-NiO and Co-decorated L-NiO exposed to 50 ppm of ethanol. (h) Sensitivity numbers of L-NiO, Fe-doped L-NiO and Co-doped L-NiO at 300, 240 and 240 ^{o}C, respectively to 50 ppm of different gases: ethanol, toluene, acetone, formaldehyde and methanol. (i) Sensitivity to various ethanol gas concentrations of L-NiO and Fe-doped L-NiO at 300 and 240 ^{o}C, respectively. (Reprinted with permission from Ref. **[95]**. Copyright 2015: American Chemical Society).

Table 2: Literature comparison on doped NiO based gas sensors with various dopants such as transition, noble metals etc**.**

Materials	Analyte gas	Gas concentration (ppm)	T_{op} (°C)	Response	Refs.
Zn-doped NiO	CO	200 400	300	-	[96]
Al-doped NiO	Ethanol	100	200	12.0	[97]
In-doped NiO	Methanol	200	300	10.9	[98]
Sn-doped NiO	Xylene	100	225	20.2	[99]
NiO activated coal	CO	100	100	125	[48]
NiO-graphene	Hydrogen	2000	350	~ 68	[100]
Cr-doped NiO	Xylene	50	325	88	[101]
Fe-doped NiO	Ethanol	100	280	~ 12	[94]
Fe-doped NiO	Trimethylamine	10	160	12.8	[102]
Ce-doped NiO	NO_2	40	150	29	[32]
Pt-doped NiO	NH_3	1000	300	1278	[103]
Au@NiO	Ethanol	100	200	2.54	[104]
W-NiO	O-xylene	15	RT	0.19	[46]
Pd-NiO	O-xylene	15	RT	0.10	
Sn-doped NiO	Xylene	1	300	65.4	[105]
Zn-doped NiO	Formaldehyde	1.4	200	136	[22]
Sn-doped NiO	Ethanol	100	340	15.6	[106]

NB. Hyphen "-" represents that the value is not reported. RT= room temperature.

5.   Effect or incorporation of transition metal dichalcogenide materials on the NiO gas sensing properties.

Transition metal dichalcogenide (TMD) monolayer are known to be atomically thin semiconductors of the type MX_2, with TMs atom M = molybdenum (Mo),

tungsten (W), etc. and a chalcogen atom X = sulfur (S), selenium (Se) or tellurium (Te), as depicted in **Figure 9a**. Our layer of M atoms is squeezed between 2 layers of X atoms, as illustrated in **Figure 9b and c**. They are part of the large family of so-called 2D nanomaterials. TMD monolayers such as molybdenum disulfide (MoS_2), molybdenum diselenide ($MoSe_2$), tungsten disulfide (WS_2) and tungsten diselenide (WSe_2) have a direct bandgap that can be used in electronics as a transistors and optics as emitters. TMD can be often being incorporated with other 2D materials such as graphene and hexagonal boron nitride. However, and these nanostructures need to be optimized correctly to be possibly used as building blocks for many various devices including sensing, transistors and other devices **[107, 108]**. Among these TMD, MoS_2 has received a great attentiveness on graphene-like 2D layered nanomaterials due to its direct bandgap of 1.8 eV and fantastic properties, which makes it to be unique and effective nanomaterial for NH_3, NO_2, H_2 and humidity detection gas sensing. It was also proven that with MoS_2 is doable to create p-n heterostructures with other SMO as an advanced type of electronic devices, providing MoS_2 sensor a potential candidate in detecting different gases at relatively low operating temperature, as illustrated in **Figure 9d** and it also depicting n-type properties due to the existence of S vacancies and strongly metal Fermi-level pinning near the conduction band edge **[109, 219]**. A typical example, Zhang et al. **[110]** showed gas sensing properties of platinum loaded cobalt oxide/molybdenum disulphide ($Pt-Co_3O_4/MoS_2$) sensor towards 1000 ppm of CH_4 gas at relative low temperature of 170 ^{o}C with a relative high response of 7.43 %. The stacking alignment of Mo and S layers of MoS_2 limit this TMD in gas sensing applications **[111 - 113]**. The MoS_2 is a lamellar nanostructure made up of three atomic layers which are joined together by weak van der Waals interaction: Mo layer squeezed

between two S layers. This interaction results in cluster phenomenon which reduces the quantity of active sites as well as the entire sensing performance. The way to maximize the amount of active sites is to functionalize or hybridize this nanostructured material with conductive templates or supports such graphene or graphene oxide whose structural stability restricts the agglomeration of MoS_2 nanoparticle, as shown in **Figure 9e – h**. One of the examples is the study reported by Venkatesan et al. **[114]** whereby reduced graphene oxide-molybdenum disulfide ($rGO-MoS_2$) sensor depicted a relatively high response of 15.6 % towards 200 ppm of H_2 at working temperature of 60 ^{o}C. Cho et al. **[115]** studied chemical sensing of 2D graphene/MoS_2 heterostructures device. The MoS_2 gas sensor detected a NO_2 gas with concentration as low as 1.2 ppm, demonstrating an extraordinary gas sensing response. The novelty on this 2D graphene/MoS_2 heterostructure based gas sensor promises to reveal uncomplicated route to crucial sensing platform for wearable electronic devices **(see Figure 9i)**.

On the other hand, WS_2 has been widely studied due to the tremendous hydrolytic characteristics as well as earth abundance. The monolayer of WS_2 has direct bandgap of 2.1 eV, due to its superb properties in optical, electrical and mechanical. This material has been substantially utilized in many fields such as gas sensors. Most of the studies have verified that WS_2 has capability to detect ammonia, nitrogen dioxide, carbon monoxide and humidity **[116, 117]**. A few examples, humidity-sensing performance of layer-by-layer self-assembled WS_2/SnO_2 nanocomposite were reported by Zhang et al. **[118]**. The WS_2/SnO_2 film sensor **Figure 10a** disclosed relatively superior sensing performance, such as unprecedented response/sensitivity, fast response rate and relatively good repeatability. The WS_2/SnO_2 film sensor exhibited a response that is 36 and 89 times

31

bigger than that of its counterpart, pure WS_2 and SnO_2 devices, respectively as illustrated in **Figure 10b**. Li et al. **[119]** showed that WS_2 sensor possessed a relatively better sensitivity and selectivity towards ammonia gas, and the response and recovery times of the sensor to 5 ppm ammonia gas are ~ 120 and 150 s, respectively. The response of the sensor improved as the humidity increased up to 73 % possibly induced by sulfides ions-assisted hydroxylation of the co-adsorbed water and oxidation of the solvated ammonia with adsorbed oxygen ions on the surface of the WS_2 nanoflakes, as illustrated in **Figure 10c and d**. Ko et al. **[120]** reported that the enhancement of gas sensing characteristics of relatively high surface area of tungsten disulfide nanosheets was induced by surface functionalization. **Figure 10e** presents the response of WS_2 nanosheets via surface functionalization by utilizing Ag nanowires, while the inset shows the Ag nanowires aligned on WS_2 nanosheets. The WS_2 based gas sensors displayed outstanding response to NO_2 gas, while imperfect recovery was noted. The WS_2 gas sensor revealed dramatically enhanced response (667 %) to 500 ppm of NO_2 exposure at the working temperature 100 ^{o}C, after silver nanowires (AgNW) functionalization. However, the nanocomposite of TMD/NiO heterojunction based gas sensors has scarcely been reported. Therefore, designing and/or fabricating a TMD/NiO based gas sensor which is capable to notice extremely fast detection with relatively low cost and power consumption, magnificent performance and with probability of integration still receives significant attention. The sensing mechanism of TMD monolayers is governed by charge transfer process **[121]**. One of the published studies by Yang et al. **[122]** revealed the sensing mechanism of n-type semiconductor MoS_2 monolayer. The charge transfer mechanisms between the oxidising (NO_2) and reducing (NH_3) gases is briefly discussed in **Figure 10f and g**. When NO_2 gas molecules are

adsorbed onto MoS_2 surface, an unpaired electron from the nitrogen atom in NO_2 normally behaves as electron acceptor, and tends to extract electrons from the MoS_2 surface, as depicted in **Figure 10f.** Therefore, such behaviour (charge transfer) causes a reduced in carrier concentration, which results to the relatively low in electrical conductivity. In a case of reducing gas NH_3 possess a lone electron pair always obeys as an electron donor, and donates its electrons to the conduction band of MoS_2. Therefore, this behaviour will result in the increase of both carrier concentration and electrical conductivity, as shown in **Figure 10g.**

The p-type WS_2 gas sensing mechanism was also explained by Yan et al. **[123]** and Xu et al. **[124]**. Initially, the p-type WS_2 sensor was introduced to the ambient air, oxygen gas molecules were adsorbed on the surface, few electrons from the valence band were extracted and oxygen (O_2^-, O^-) species was created, resulting to an increase and decrease in hole concentration and resistance, respectively, as illustrated in **Figure 10h**. During the exposure of oxidising gas, NO_2 gas molecules were adsorbed as NO_2^- ions, moreover withdrew electrons from the valence band and enhanced the hole content which result in an increased in electrical conductivity. The formation of a hole-accumulation layer at the facet of WS_2 by chemisorption of NO_2 was seen in **Figure 10i**. Consequently, creation of more holes caused the p-type WS_2 become more conductive as presented in **Figure 10j**. In the case of reducing gas, the opposite happened. The NH_3 donates electron to the WS_2 material and decreased the hole concentration which result in a decreased in an electrical conductivity **[120]**. The concept of gas sensing mechanism for p-n heterojunction is briefly discussed in section 8.
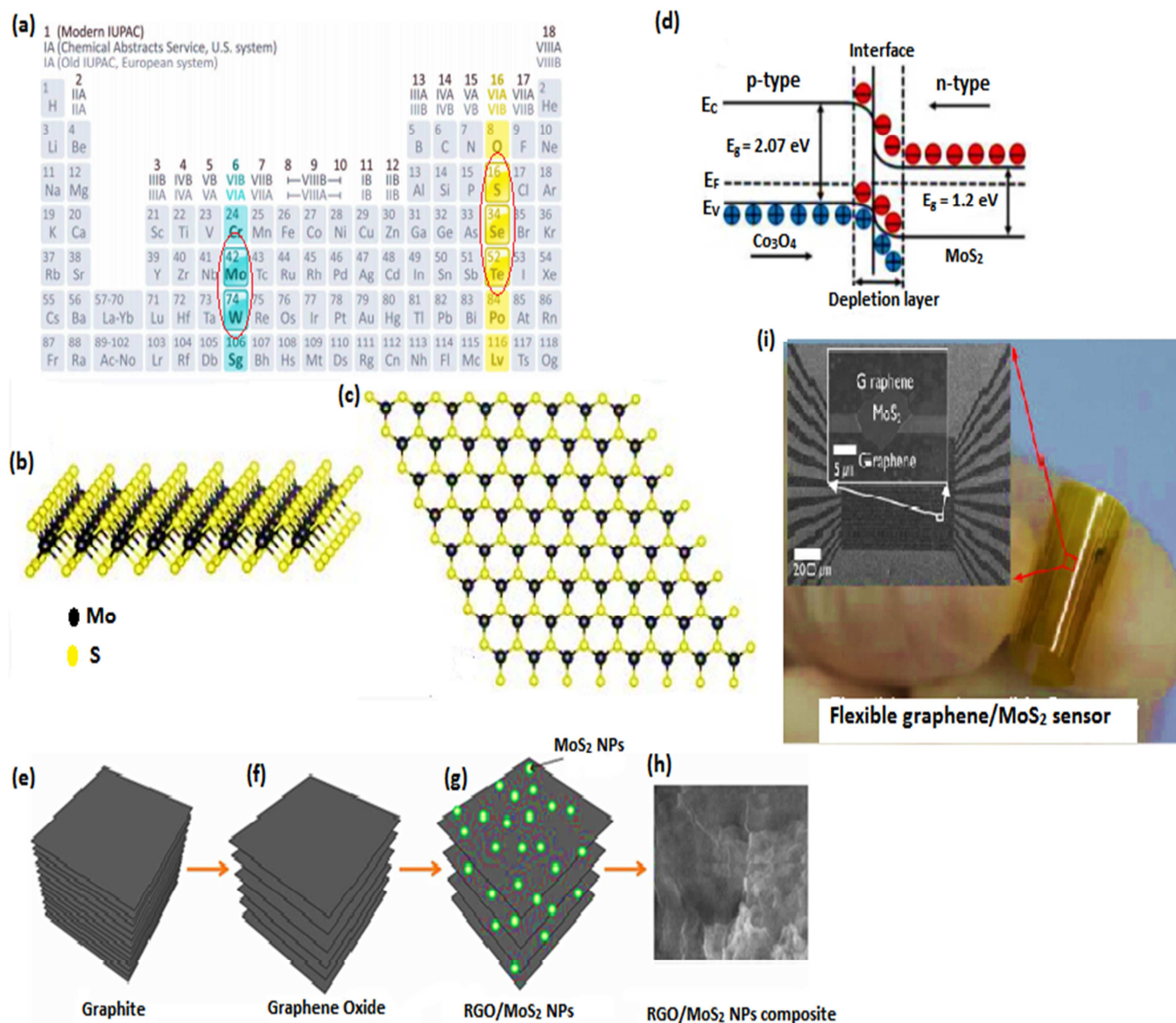
Figure 9: (a) TMD elements highlighted and circled in periodic table. (b) Structure of a hexagonal TMD monolayer and (b) top view of hexagonal TMD monolayer (Mo and S atoms are in black and yellow, respectively) (Reprinted with permission from Ref. **[108]**. Copyright 2018: RSC journal). (d) Schematic representation of Co_3O_4 and MoS_2 p-n heterojunction. (Reprinted with permission from Ref. **[110]**. Copyright 2017: Elsevier). Schematic diagram of fabrication of rGO/MoS_2 nanocomposite sensing layer (e) graphite, (f) graphene oxide (GO) synthesized by modified hummer's method, (g) rGO/MoS_2 nanocomposite and (h) FESEM micrographs of RGO/MoS_2 composite. (Reprinted with permission from Ref. **[114]**. Copyright 2017: IOP Publishing). (i) Actual picture of a graphene/MoS_2 heterostructured device on a curved polyimide substrate and inset shows the FESEM image of graphene/MoS_2 sensor. (Reprinted with permission from Ref. **[112]**. Copyright 2018: Elsevier).
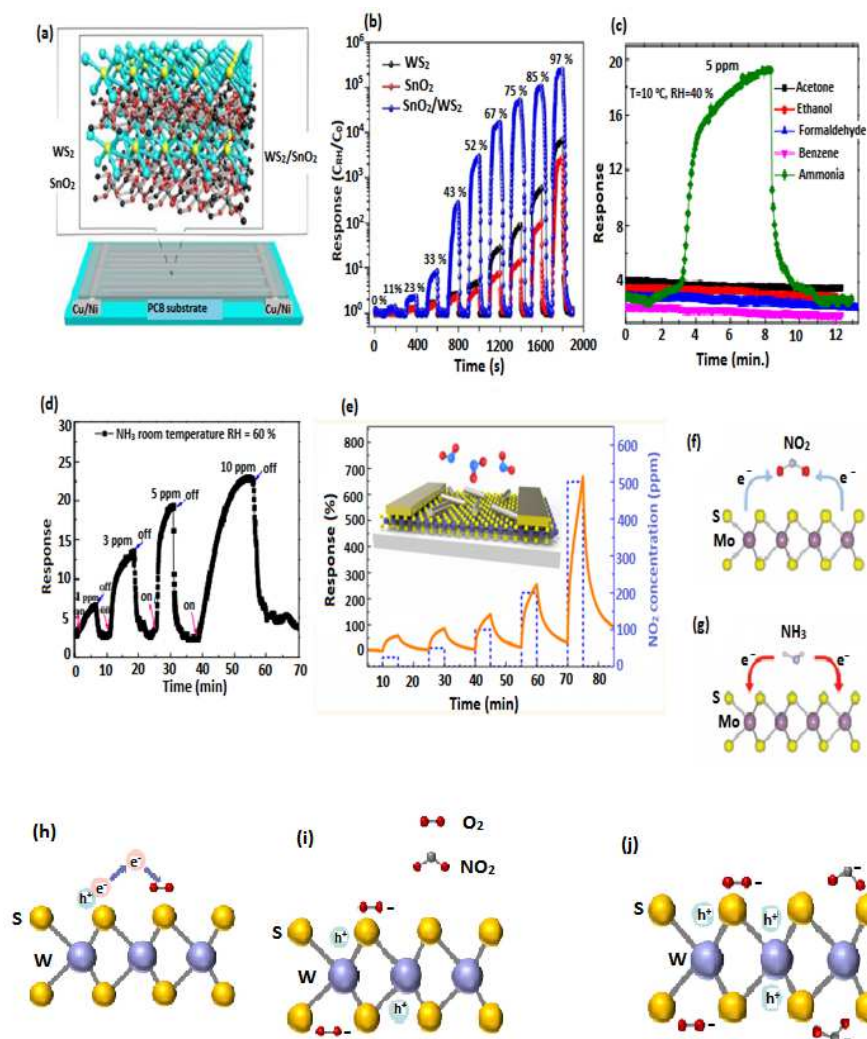
Figure 10: (a) Schematic illustration of layer-by-layer self-built WS_2/SnO_2 nanocomposite sensor. (b) The response of different gas sensors: pure (WS_2 and, SnO_2), and WS_2/SnO_2 nanocomposite towards humidity. (Reprinted with permission from Ref. **[118]**. Copyright 2018: Elsevier). (c) The selectivity of the WS_2 gas sensor towards various gases at RH = 40 %. (d) The dynamic response curve of the WS_2 gas sensor with ammonia gas concentration in the range of 1 to 10 ppm. (Reprinted with permission from Ref. **[119]**. Copyright 2017: Elsevier). (e) The response of WS_2 nanosheets via surface functionalization by utilizing Ag nanowires and the inset of Ag nanowires aligned on WS_2 nanosheets. (Reprinted with permission from Ref. **[120]**. Copyright 2016: American Chemical Society). Schematic diagram of the charge transfer mechanisms for MoS_2 during the exposure of (f) NO_2 oxidising gas and (g) NH_3 reducing gas. (Reprinted with permission from Ref. **[122]**. Copyright 2016: Royal Society of Chemistry). (h) Sketch of the gas sensing mechanism for p-type WS_2 towards NO_2 gas molecules, formation of chemisorbed ion O_2^- on the surface of WS_2 nanosheets during the exposure of ambient air. (i) The hole content enhanced after the formation of O_2^- and (j) the induced improving hole content by chemisorption of NO_2 gas. (Reprinted with permission from Ref. **[124]**. Copyright 2018: Elsevier).

6. Effect of conducting polymers on the NiO gas sensing characteristics.

Conducting polymers are the conjugated polymers consist of π-bonds on their backbone, which assists in the movement of electrons through the polymeric chain. These conducting polymers are considered as the promising materials that can behave as conductors, semiconductors, superconductors and magnetic materials. The role of delocalized π electrons on the backbone of these conducting polymers persuades the unique optical and electrical properties **[125 - 127]**. Up to date, the conducting polymers including polypyrrole (PPy), polyaniline (PANI), poly(3-hexylthiophene) (P3HT), poly(3,4-ethylenedioxythiophene) (PEDOT) and polythiophene (PTh) are the most studied polymer materials, particularly in the gas sensing applications. The various conducting polymers with their electrical conductivities are shown in **Table 3**. Previous studies have indicated that these conducting polymers, particularly after significant doping, are favourable materials for detecting volatile organic compounds (VOCs) in a room temperature. However, there are different parameters that can influence polymer films response to organic vapour such as description of the solvent from which the film was initially grown and the nature of anion which is doped **[128 - 130]**. Generally, most of the gas sensors available are SMO which operate at relatively elevated temperatures. This generates structural modifications in the sensing material resulting to an instability and response variation. Additionally, another risk with regard to the detection and/or identification of combustible gases or gas mixture at relatively high temperatures is that they might auto-ignite. The polymer based gas sensing materials allow a safer detection of a several gases in an ambient conditions i.e. room temperature. The incorporation of polymer materials into the SMO based sensors can be used to

improve gas sensing characteristics. Furthermore, this can be utilized to induce the sensitivity and selectivity of organic based gas sensors **[131]**.

**Table 3:** The electrical conductivities of different conducting polymers.

Conducting polymers	Conductivity S/cm
PANI	$10^{-10} - 10^3$
PPy	$10^{-5} - 10^3$
PTh	$10^{-4} - 10^3$
P3HT	$10^0 - 10^2$
PEDOT	$10^{-6} - 10^3$

A typical example, Das et al. **[132]** reported one-pot synthesis of ZnO-PANI nanocomposite for fabrication of efficient room temperature ammonia gas sensor. They illustrated that ZnO-PANI is highly selective for NH_3. Xie et al. **[133]** reported organic thin film transistor (OTFT) gas sensors based on poly (3-hexylthiophene-2,5 diyl) (P3HT)-MoS_2 nanocomposite film depicted a relatively shorter recovery time (500 s) compared to its counterparts when the ammonia gas concentration varied in the range of 4 to 20 ppm. The charge transfer in the nanocomposite system is controlled by various possible paths, such as the charge transfer between the polymer chains by hopping, hopping between the polymer chains and a single-layer MoS_2, and hoping between the MoS_2 via the polymer chains. The extremely quick charge transport was achieved by a closer interlayer d-spacing and better π - π stacking of the P3HT chains. According to the reports, they are few studies on the composite of NiO and conducting polymers based gas sensors. However, an establishment of Nalage et al. **[134]** on PPy-NiO hybrid nanocomposite indicated that the electrical conductivity of PPy enhances drastically after the incorporation of

NiO into PPy matrix, as shown in **Figure 11a and b**. This behaviour was noticed because PPy, NiO and PPy-NiO nanocomposites are all p-type semiconductors. Therefore, these nanomaterials are consisting of relatively large amount of free charge carriers unoccupied for the intention of conduction. The amount of NiO is proportional to the quantity of charge carriers, implying that, as content of NiO improved the free charge carriers are also enhances. All the electrons from polar O^{2-} aborted NiO nanoparticles surface and from the PPy chains lead to their amplification in the electrical conductivity of PPy-NiO hybrid nanocomposite.

Nalage et al. **[135]** reported an NO_2 gas sensor based on polypyrrole-NiO nanocomposite films as illustrated in the micrographs of (c) PPy, (d) NiO and (e) PPy-NiO (50%) nanocomposite in **Figure 11**. The PPy-NiO nanocomposite in **Figure 11f** revealed a response of approximately 47 towards 100 ppm NO_2 compared to response values of 36 and 13 for pure PPy and NiO, respectively. The observed higher response is due to that NiO and PPy possess p-type semiconducting characteristics as mentioned before, and NO_2 is a typical electron-accepting gas molecule, resulting to an enhance of hole concentration in the nanocomposite, refer to **Figure 11g**. Nalage et al. **[136]** reported that the response of the camphor sulfonic acid (CSA)-doped PPy –NiO hybrid sensor towards 100 ppm NO_2 was twice bigger than that of pure PPy, as shown in **Figure 11h**. The response and recovery times were decreased drastically compared to its counterparts PPy and PPy-NiO sensors, as illustrated in **Figure 11i and j**. The improved gas sensing performances were attributed to the change in morphology and activity of CSA with PPy and NiO. The addition of CSA modified the structural properties and chemical nature of polymer nanocomposite by producing more active centres for adsorption of gas molecules. Polymer based gas sensors and/or polymer-SMO gas sensors are more

advantageous than MOX based gas sensors due to the fact that they can be operated in relatively low temperatures this restrict structural changes of the material, reduces the power consumption and allows low-risk detection of combustible gases.
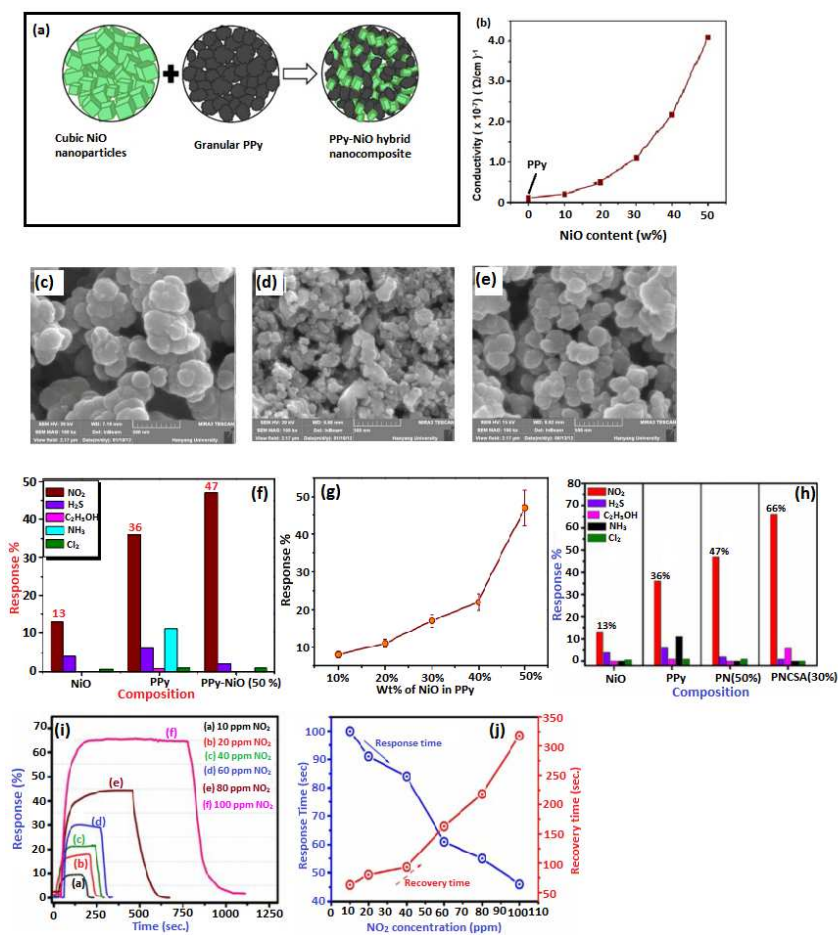
Figure 11: (a) Schematic diagram of the fabrication of PPy-NiO hybrid nanocomposite. (b) A line graph of conductivity against NiO quantity in PPy matrix. FESEM micrographs of (c) PPy, (d) NiO and (e) PPy-NiO (50%) hybrid nanocomposites. (f) The selectivity of PPy, NiO and PPy-NiO (50 %). (g) The response of PPy-NiO (10 – 50 %) hybrid gas sensor to 100 ppm NO_2. (Reprinted with permission from Ref. **[134]**. Copyright 2013: Elsevier). (h) The bar graph of response against composition of NiO, PPy, PPy-NiO and PNCSA sensors. (i) Response vs time plots for PNCSA sensor for various concentrations of NO_2 gas. (j) The response and recovery time periods of PNCSA sensor against NO_2 concentration. (Reprinted with permission from Ref. **[135]**. Copyright 2014: Springer nature).

7. Effect of phosphors materials on the NiO gas sensing features.

Phosphors are solid luminescent nanomaterials that release photons under excitation induced by external energy source, such as electron beam, ultraviolet (UV) light or any wavelength of light in the electromagnetic (EM) spectrum range. Additionally, most of the phosphors nanostructured materials are activated with rare earth (RE) ions **[137 - 139]**. These RE ions are sequence of 15 elements in the periodic table arranged from lanthanum to lutetium. The $4f^n$ electrons shell structure of all trivalent ions in their electronic arrangement $[Xe]4f^n$, are packed gradually from n = 0 to 14 electrons and are protected by packed $5s^2$ and $5p^6$ electrons shells so that the 4f electrons are less affected by environment surroundings **[140]**. These RE based phosphors materials can be categorised into two types: broad band and narrow band emissions assigned to the d→f and f→f transitions, respectively. The widely used RE ions are europium (Eu^{3+}/Eu^{2+}), cerium (Ce^{3+}), terbium (Tb^{3+}), gadolinium (Gd^{3+}), ytterbium (Yb^{3+}), dysprosium (Dy^{3+}), thulium (Tm^{3+}), erbium (Er^{3+}) etc. The RE based phosphors have shown various applications, due to their remarkable technological significance including solid state lighting, medical labelling, imaging, radiation detection, gas sensors, etc. **[141]**.

In gas sensing applications, studies have revealed that the RE elements and/or rare earth oxide (REO) can be potential candidates for enhancing sensing performances due to their rapidly oxygen ion mobility, effective catalytic nature and large surface basicity **[142]**. A few examples, Hastir et al. **[143]** reported the temperature dependent selectivity performance of Er and Tb doped ZnO sensors to ethanol and acetone gases. Giang et al. **[144]** studied hydrocarbon gas sensing of nano-crystalline perovskite oxides $LnFeO_3$ (Ln = La, Nd and Sm). Anbia et al. **[145]** reported humidity sensing features of Ce-doped ZnO thin film sensors synthesized

by sol-gel technique. Dong et al. **[146]** disclosed a Dy_2O_3 sensor with highly sensitivity, relatively good selectivity and reproducibility to NH_3 gas at room temperature. There are numerous reasons leading to the enhanced gas sensing properties such as more 4f electrons in Dy_2O_3 REO and this supplies more accessibility for oxygen molecules to transform reactive oxygen species. Koshizaki et al. **[147]** investigated sensing characteristics of ZnO-based NO_x sensor. These results indicated that the addition of RE elements such as Er, Tm, Yb and lutetium (Lu) enhanced the sensitivity and selectivity to NO_2 against NO. Bano et al. **[148]** reported a selective detection of NO_2 gas based on nickel copper oxide incorporated with RE. Hastir et al. **[149]** showed that the pure ZnO sensor was highly sensitive to 50 ppm ethanol with the response of 48 at working temperature of 280 ^{o}C, while its counterpart Tb^{3+}-doped ZnO sensor revealed the maximum response of 48 to 50 ppm of acetone at operating temperature of 400 ^{o}C. The improved sensing behaviour is due to catalytic nature, relatively big surface basicity and fast oxygen ion mobility. This catalytic nature of RE elements and/or REO can therefore enhance the rate of reaction by supporting a various reaction path possessing relatively lower activation energy. In principle, the most of the SMO gas sensors are operated at relatively high temperature, this means high activation energy is desired for reaction including analyte gas species and adsorbed oxygen ions leading in a precondition of elevated temperature, while for RE based gas sensors, a path of lower activation is offered by the catalytic activity of RE dopant thus assisting in achieving high sensitivity at relatively lower operating temperature **[150]**.

Gawali et al. **[151]** revealed that different gases such as liquefied petroleum gas (LPG), NH_3, acetone (CH_3COOCH_3) and NO_2 were examined by Ce doped NiO based gas sensor, see **Figure 12a - d**. Among all other gases, the maximum

sensitivity towards NO_2 was achieved in around 0.719 % per ppm at an average temperature of 150 ^{o}C. The improvement in gas sensing characteristics for Ce doped NiO was assigned to the deformation of crystal structure induced by incorporation of Ce into NiO. This deformation was confirmed by XRD results in **Figure 12a,** since the diffraction peaks shifted to the lower Bragg's angles, this suggested the lattice expansion. This is due to that the ionic radii of Ni^{2+} and Ce^{3+} are respectively 69 and 101 pm. The larger ionic radius of Ce^{3+} could cause a stress and strain in a crystal structure of NiO. **Figure 12b and d,** indicated that Ce-doped NiO sensors were highly selective to the NO_2. **Figure 12c** presents a temperature dependence studies of NO_2 (at 40 ppm) sensitivity for Ce-doped NiO. The findings displayed a high sensitivity at relatively low temperature and sensitivity reduced drastically at relatively high temperatures. This decrease was caused by the quantity of adsorbed NO_2 on Ce-doped NiO surface decreases. In addition, the NO_2 gets reduced to NO at elevated temperatures leading to the decrease in sensitivity. The highly porous and larger surface area of the NiO contributed to this enhanced gas sensing properties, because more NO_2 gas molecules were adsorbed on the facet as well as in the internal portion of the samples. On the other hand, Farghali et al. **[152]** studied synthesis and multi-functionality of CeO_2-NiO nanocomposites synthesized via sonochemical method. The surface areas of 69.571, 32.56 and 38.52 m^2g^{-1} were achieved for NiO, CeO_2 and CeO_2-NiO nanocomposite, respectively, due to the various morphology in **Figure 12e – g**. The oxygen vacancies generated in CeO_2 when some oxidation state of Ce^{3+} changed to Ce^{4+} provides very pleasing sites for gas adsorption. Mrabet et al. **[153]** showed that the electrical conductivity increased during the incorporation of lanthanum (La) into a NiO because La^{3+} ions replaced Ni^{2+} ions. The extrinsic conduction is more dominate than the intrinsic conduction.

Therefore more impurities or vacancies exist in the La-doped NiO material assist to generate free carriers. Therefore, the presence of $LaNiO_3$ also plays an exceptional role in the enhancement of the electrical conductivity.
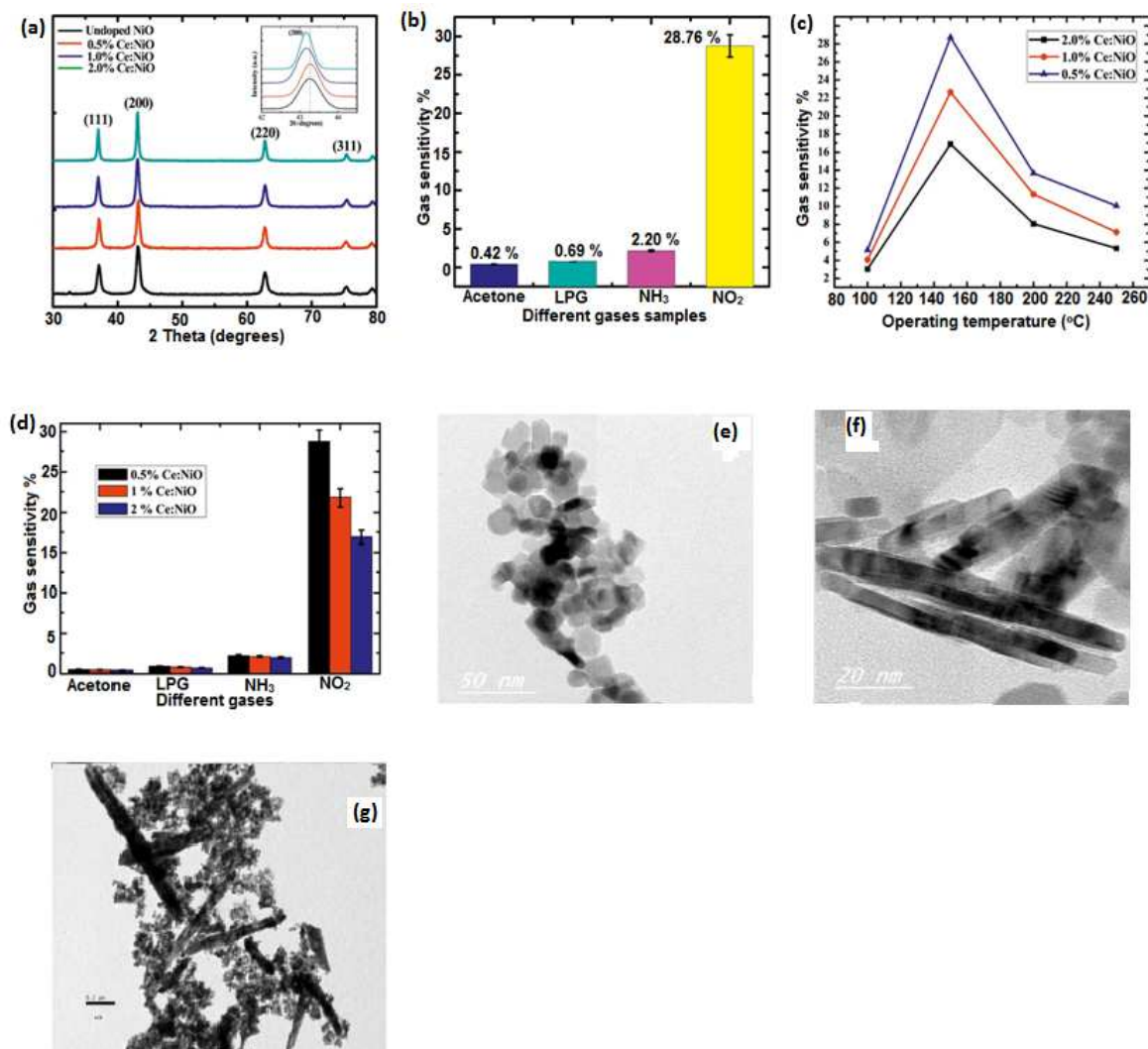

Figure 12: a) XRD analysis of Ce-doped NiO. (b) The selectivity of Ce-doped NiO gas sensor towards different gases. (c) Gas sensitivity against various operating temperature at 40 ppm of NO_2 gas for all doped Ce - NiO sensors, (d) The bar graph of selectivity against compositions of Ce-doped NiO sensors toward different gases. (Reprinted with permission from Ref. **[151]**. Copyright 2018: Elsevier). TEM images of (e) CeO_2 nanoparticles, (f) NiO nanorods and (g) CeO_2-NiO nanocomposite. (Reprinted with permission from Ref. **[152]**. Copyright 2018: Elsevier).

8. Influence of zero, one, two and three dimensional heterostructures on the NiO gas sensing characteristics.

Heterostructures fabricated by low dimensional building blocks such as particles, sheets, wires, rods, tubes, or cones have appealed the attention researchers for the previous years due to their distinctive properties **[154]**. The preparation of zero-dimensional (0D), one-dimensional (1D), two-dimensional (2D) and three-dimensional (3D) nanostructured materials has shown remarkable properties in various fields, especially in gas sensing applications. For instance, in 0D nanomaterials all dimensions are within the range of nanoscale and these nanomaterials include quantum dots and nanospheres, as illustrated in **Figure 13a and b**. The micrographs of 1D nanostructure such as nanowires and nanorods are depicted in **Figure 13c and d**, and these 1D nanostructures have only two dimensions in a nanoscale range. In 2D nanostructures only one dimension is within the range of nanoscale and these nanostructures include nanoplates and nanodisks, as shown in **Figure 13e and f**. Additionally, these 2D nanostructures are considered as the building blocks for the key constituent of nanodevices for application perspective. On the other hand, 3D nanomaterials has attracted intensive research interest due to the fact that the nanostructured materials have relative large surface area and provide sufficient adsorption sites for all included gas molecules in a small space. The other factor that contributes to the 3D nanomaterials is a porosity which can lead to the better transport of molecules. The 3D nanostructure features also in a form of nanocones and nanoflowers, as depicted in **Figure 13g and h [155]**. Several studies have reported that the preparation of MOX and/or heterostructures with various morphologies is very crucial in the field of gas sensing, refer to **Figure 2a**. **Figure 14** presents the hierarchical nanostructures associated to the dimensions

44

of the nanobuilding blocks. The hierarchical nanostructure simply implies the bigger dimension of nanostructure is made up of many, low dimensional, nanobuilding blocks. These hierarchical nanostructures possess non-linear shapes that are normally developed from atoms, molecules or particles in 2D or 3D and in non-equilibrium growth mechanisms **[156]**. The 1-3 urchin are the 1D nanowires/nanorods that are fabricated into a 3D urchin-like spherical shape and 2-3 flower in **Figure 14** demonstrates the 3D flower-like hierarchical nanostructure that is constructed from many 2D nanosheets. The hollow-spheres are considered as the gathering of 1D nanoparticle into the 3D hollow spherical shape. The 1-3 hollow urchin and 2-3 hollow flower nanostructures illustrated in **Figure 14 [157 - 159]**.
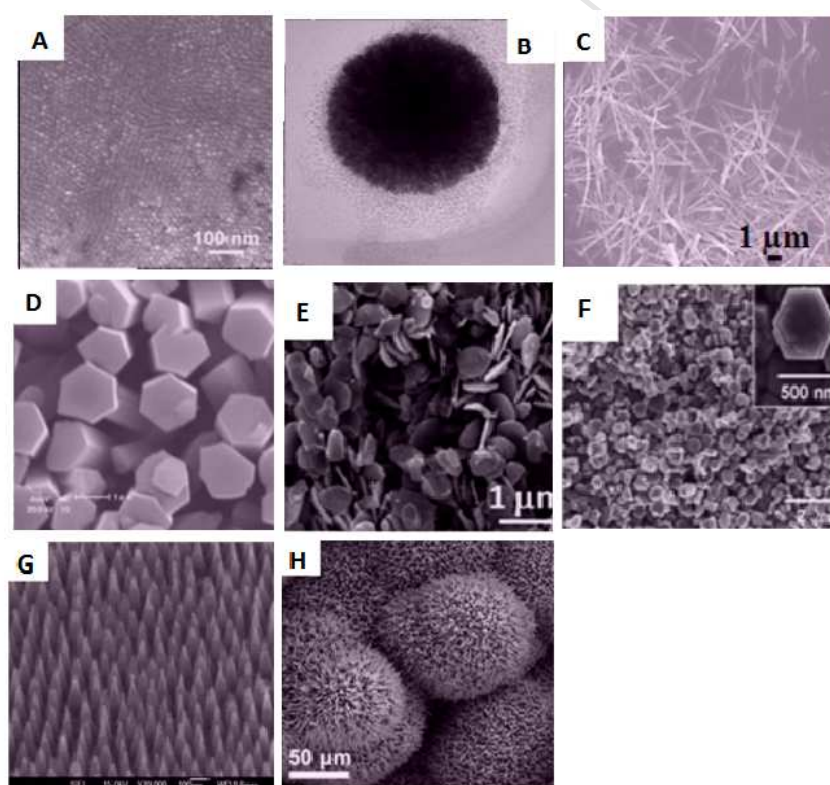
Figure 13: TEM and SEM micrographs of (a) quantum dots, (b) nanospheres, (c) nanowires, (d) nanorods, (e) nanoplates, (f) nanodisk, (g) nanocones, (h) nanoflower. (Reprinted with permission from Ref. **[155]**. Copyright 2012: Elsevier).

Figure 14: Naming of hierarchical nanostructures related to the dimensions of the nano-building blocks and of the consequent hierarchical nanostructures**.** (Reprinted with permission from Ref. **[159]**. Copyright 2009: Elsevier).

0D hollow nanospheres have proved to have relatively good sensing properties due to their relatively high surface area, structural stability and catalytic activity. From nanoscience and nanotechnology perspective it is known that when combining nanomaterials with other different form of 0D MOX, the newly formed

heterostructures with unique properties, significantly enhances the gas diffusion along the layers and hence provides the nanocomposite with better sensing performance. These heterostructures are very important due to their effective band reassemble in the heterojunction which plays an impressive role in adjusting the charge transfer path and the resistance of the sensing layer **[160]**. For example, Ju et al. **[161]** disclosed that triethylamine (TEA) gas sensor with relatively high response and selectivity prepared successfully in a p-n heterostructure composed of n-type SnO_2 hollow spheres and p-type NiO nanoparticles. These two sensors, NiO/SnO_2 and SnO_2 demonstrated a rapid response towards the target gas TEA with the response and recovery times of approximately 11 and 6 s, respectively. **Figure 15a** presented that the recovery of NiO/SnO_2 sensor was very long (T_{rec} =34 s) compared to the SnO_2 sensor (T_{rec} =25 s). In **Figure 15b** the bar graph depicted that the NiO/SnO_2 sensor was greatly selective to the TEA gas with the response value of 48.7, amongst all other tested gases such as acetone, benzene, and xylene.

In n-type SnO_2 and p-type NiO major carriers are electrons and holes, respectively. When these two nanomaterials combine as shown in **Figure 15c** the respective majority carriers of both semiconductors diffuse in the different directions due to their differentiation in work function until the equilibrium in Fermi levels (E_f) is achieved. This causes the generation of p-n heterojunction with the energy band in the interfaces of semiconductors. At relatively high temperatures, when the sensor with p-n heterojunction exposed in air the resistance of the composite in air (R_a) will be relatively higher than SnO_2 due to the depletion region at the heterojunction interface. The formation of depletion layer on the surface of SnO_2 is due to the chemisorbed oxygen ions which extracts electrons. This further increases the resistance of composite in air. In p-type NiO the opposite behaviour occurs

compared with the n-type SnO_2. A hole accumulation layer is formed because oxygen is extracting the electrons from the surface, introducing more holes resulting in the low resistance of the NiO layer. The resistance is more dominated by the surface of SnO_2 and depletion regions on the heterojunction interface. Once the SnO_2/NiO heterojunction sensor exposed to the reducing gas TEA, the chemisorbed oxygen ions interact with TEA gas molecules and donate electrons back to the SnO_2, inducing the decline in depletion regions, therefore the reduce of nanocomposite resistance, as illustrated in **Figure 15d**. The TEA gas molecules provide electrons to fill the holes in the p-type NiO, resulting to the drop in holes concentration. Hence, the diffusion of carriers is minimized and the depletion layer is also reduced. It is evident from semiconductor theory that the resistance (R) of the sensor strongly depends on the potential barrier height related to the following equation [162]:

$$R = R_o \exp(^{qV}/_{kT}) \tag{14}$$

where R_o, q, V, k and T is the initial resistance, charge of an electron, potential energy barrier height, Boltzmann's constant and absolute temperature of the sensing material, respectively. The response is affected by the small variation in the potential barrier height at the interface. Hence, the improved response of the heterostructure sensor compared to its counterpart SnO_2 is partially assigned to the modification in the potential barrier height at the NiO/SnO_2 interface **[163]**. Conclusive remarks can be drawn that, the origination of p-n heterojunction at the interface of nanocomposite sensor enhances the resistance in air and decrease the resistance in TEA gas. Therefore, the response towards TEA gas is enhanced due to differences in resistance.

Bai et al. **[164]** showed that the NiO@ZnSnO$_3$ p-n heterojunction sensor has relatively high response of 2.2 and 10.4 towards 0.1 and 1.0 ppm formaldehyde gas, respectively. Kim et al. **[165]** showed that NiO/NiWO$_4$ sensor has a relatively better response of 343.5 towards 5 ppm p-xylene compared to the pure NiO sensor. This good sensing performance was attributed by large surface area, chemiresistive variation due to the development of p-n heterojunction and synergistic catalytic activity between NiO and NiWO$_4$.
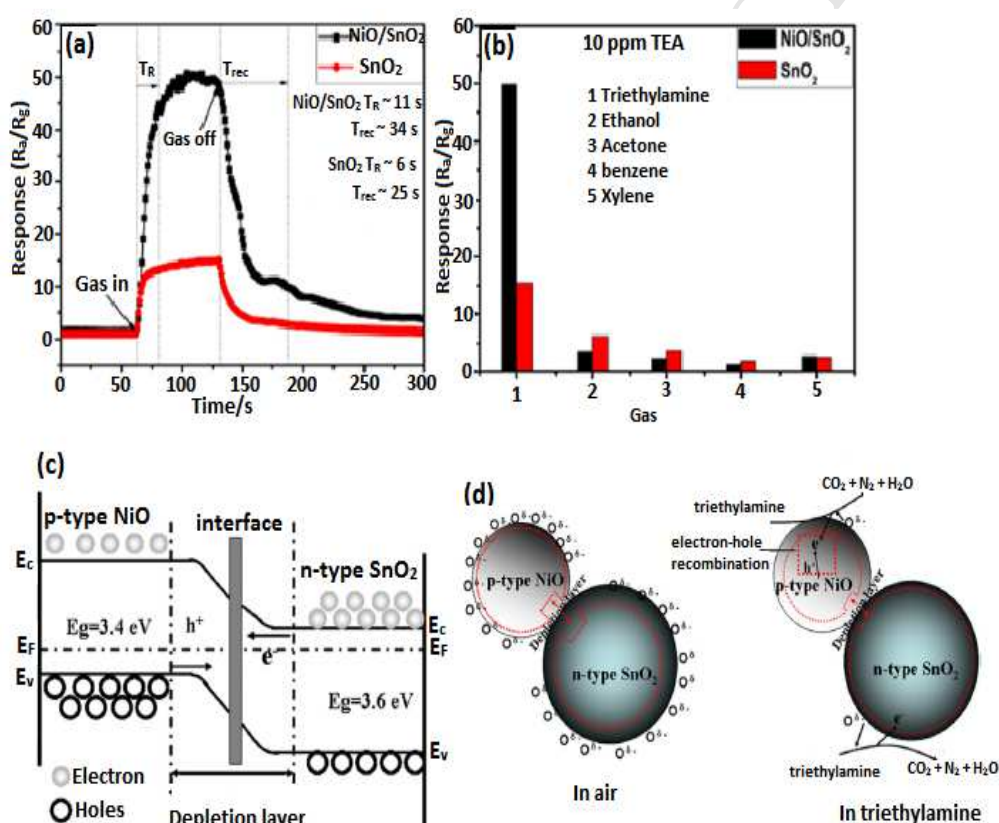
Figure 15: (a) Response-recovery curve of p-n NiO/SnO$_2$ sensor to 10 ppm TEA at operating temperature of 220 $^{\circ}$C, (b) Selectivity of sensors towards various gases with similar concentration at working temperature 220 $^{\circ}$C. (c) Schematic diagram depicting energy band structure of p-NiO/n-SnO$_2$ heterostructures, (d) A model of NiO/SnO p-n heterostructures exposed to air and TEA gas. (Reprinted with permission from Ref. **[161]**. Copyright 2015: Elsevier).

1D heterostructures such as nanorods, nanowires and nanobelts have been described with at least one spatial dimension in the range of 1 – 100 nm. However, the fundamentals of gas sensing mechanism which includes adsorption and desorption remains unchanged, but 1D heterostructures based gas sensors offer many fascinating features such as (i) ultra-sensitivity and rapidly response time, (ii) relatively higher selectivity and stability, (iii) light weight and low power consumption and (d) relatively low-temperature operations [166]. In additional, the 1D heterostructures based gas sensors are widely used because of the speedy charge transfer throughout a one direction of the crystallized nanostructures. There are mostly common factors strengthening the enhancement of gas sensing characteristics such as structural defects related to oxygen vacancies, relatively large active surface area for adsorption and desorption and the resistance variation due to the formation of heterostructures [167]. A typical example, Sun et al. [168] showed that TiO_2 and NiO-decorated TiO_2 nanorod sensors has the responses of ~ 5.76 and 9.33, respectively towards 200 ppm acetone gas at working temperature of 400 ^{o}C. Zheng et al. [169] designed the sensors from NiO-doped SnO_2 nanofibres and a relatively good formaldehyde sensing characteristics at working temperature of 200 ^{o}C, and the minimum detection limit of 0.08 ppm was observed. The response and recovery times of the sensor were about 50 and 80 s to 10 ppm formaldehyde gas, respectively. Another type of heterostructures of NiO@ZnO heterostructured core-shell nanoparticles (NPs) and nanotubes (NTs) was also studied by Xu et al. [170] prepared through coelectrospinning revealing enhanced gas sensing properties. A response of the relatively best NiO@ZnO nanotubes sensor to 50 ppm H_2S gas enhanced as maximum as 2.7 – 23.7 times compared to other sensors. These improved gas sensing characteristics were assigned to the alteration of

50

nanostructures and ZnO activity and NiO nanocrystals as well as association of homo- and heterointerfaces. Li et al. **[171]** studied electrospun nanofibers of p-type NiO/n-type ZnO heterostructure with various amount of NiO and its impact on TMA sensing characteristics. Their findings demonstrated that the NiO/ZnO nanofibers has significantly increased response, relatively good selectivity towards TMA and rapidly response and recovery times roughly 30 and 35 s, respectively.

Wang et al. **[172]** reported electrospun nanowebs of NiO/SnO_2 p-n heterojunctions which were successfully prepared using electrospinning method followed by thermo-compression and subsequent calcination process. The response of the p-n heterojunction sensor (R_a/R_g = 27.5) was 1 order of magnitude relatively bigger than that of its counterpart, pure SnO_2 nanowebs towards 100 ppm ethanol gas with an average response and recovery times of ~ 2.9 and 4.7 s, respectively. Baratto et al. **[173]** reported the bottle-brush-shaped heterostructures of ZnO-NiO nanowires analysed towards various gases such as acetone, ethanol, NO_2 and H_2. Furthermore, these sensors continued to maintain n-type gas sensing mechanism, with the enhanced sensing performance due to high catalytic action of NiO. The sensing mechanism is strongly influenced by the existence of NiO-ZnO p-n heterojunction with a relatively less response and recovery times towards 100 ppm of ethanol gas at working temperature of 500 ^{o}C with the response of 95. Wang et al. **[174]** studied the NiO/SnO_2 p-n heterojunction sensors that were spin-coated on the ceramic tube coupled with Au electrodes for the detection of hydrogen target gas. A rapid response-recovery times behaviour (~ 3s) at a working temperature of 320 ^{o}C, with the detection limit of roughly 5 ppm H_2 were achieved. Zhang et al. **[175]** demonstrated that the porous $NiO-WO_3$ composite nanofibers displayed a relatively higher sensitivity, fast response, and relatively small recovery time towards acetone

gas. These unique properties were justified as outstanding pores and uneven and/or irregular surface structural properties. The role of relatively big pores causes the oxygen and acetone gas molecules to diffuse rapidly to the sensing layer, resulting to the speedy response and recovery times. Secondly, more oxygen gas molecules can be adsorbed and ionized due to the relatively large surface area and small particle size of p-n heterojunction NiO-WO$_3$ sensors. Haq et al. **[176]** showed that the sensing response of Fe$_2$O$_3$/NiO nanosheet-covered fibers were 18.24 toward 100 ppm acetone gas at operating temperature of 169 ^{o}C, and this response was 6.9 times bigger than that of pure NiO nanofibers. The enhanced gas sensing properties on Fe$_2$O$_3$/NiO was associated with the morphology with relatively large surface area, interface in p-n heterojunction and synergetic performance of Fe$_2$O$_3$ and NiO**. Figure 16** presents SEM micrographs of nanocomposites on Fe$_2$O$_3$/NiO fibers assembled with nanosheets (a) low and (b) high magnification. **Figure 16c** presents the schematic illustration of acetone sensing mechanism on the heterostructure sensors of Fe$_2$O$_3$/NiO nanosheet-covered fibers in the existence of air and acetone analyte gas. The energy band configuration of NiO and Fe$_2$O$_3$ with the experimental energy bandgap of 3.37 and 2.05 eV, respectively, in air before combination, is shown in **Figure 16d**. The energy band arrangement of the nanocomposites based on Fe$_2$O$_3$/NiO p-n heterojunction in acetone is depicted in **Figure 16e**. This gas sensing mechanism is similar to the one explained previously in 0D heterostructures by Ju et al. **[161]**, the only difference here is geometry of 1D heterostructure, but the concepts is the same. Chao et al. **[177]** reported that the NiO-In$_2$O$_3$ nanofibers sensor depicted good selectivity and stability to 100 ppm ethanol gas at working temperature 300 ^{o}C. Generally, the enhancement in gas sensing features for SMO, particularly to the 1D heterostructures, can be assigned to the construction of p-n

junction between NiO and In_2O_3, high potential of adsorbed oxygen species and large surface area.

Recently, mono- or few layer 2D heterostructure materials which include nanoplates, nanodisks and nanosheets as a new classification of room temperature gas sensing materials have attained more special recognition, owing to their fantastic chemical and physical features, such as relatively high active surface area for the adsorption of gas molecules, low electrical noise and high conductivity **[178 - 180]**. In additional, the 2D nanomaterials possess a great bright future in the progress of ultrahigh sensitive and low-power utilization sensor platforms **[181]**. The sensing mechanism of typical 2D layered nanostructured materials particularly graphene is governed by charge transfer process. In this section, we briefly described the current trends of NiO-based 2D heterostructures or nanocomposite films for gas sensors **[182 - 184]**. A typical example, Gaspera et al. **[185]** investigated Au nanoparticles in TiO_2-NiO films for surface plasmon resonance (SPR) based and selective H_2S gas sensing. The detection sensitivity is demonstrated to be relatively low to a few ppm of H_2S, and almost no disturbance in response is noticed during simultaneous exposure to CO or H_2S, leading to a highly sensitivity and selectivity towards H_2S gas. The radio frequency (RF) sputtered SnO_2/NiO thin films were investigated at sub-ppm H_2S sensor at room temperature by Kaur et al. **[186]**.

Figure 17 presents a schematic diagram of sensing component (a) film side, (b) Pt-100s connected on the rear side of sensor component and real images of (c) sensor film on a Teflon head (d) sensor with Teflon head attached to a circuit with a temperature controller. While a selectivity histogram of pure SnO_2, NiO and p-n SnO_2:NiO gas sensors toward various gases at room temperature is shown in **Figure 17**e. Among the various monitored gases such as NO, NH_3, C_2H_5OH, CO,

53

H$_2$S and CH$_4$, all the sensors depicted the highest response toward H$_2$S. **Figure 17f** presents a sensor response against the working temperature of NiO, SnO$_2$ and SnO$_2$:NiO gas sensors towards 10 ppm H$_2$S gas. The sensor response demonstrated by NiO/SnO$_2$ thin film is 9 and it is 415 times more than that revealed by pure NiO and SnO$_2$ films, respectively. The improvement on these gas sensing characteristics of SnO$_2$:NiO p-n heterostructures is ascribed to various mechanisms- (i) oxidation reaction between adsorbed oxygen gas and H$_2$S analyte gas and (ii) demolition of p-n heterojunctions due to translation of NiO to metallic nickel sulphide i.e. ultimate product of NiO when reacted with H$_2$S. Furthermore, since it is very popular that the response and/or sensitivity of p-type is the square root of n-type SMO with the similar morphology, therefore, the improvement in response and/or sensing features is due to the p-n heterostructures, the synergistic behaviour between the metal oxides played a vital role in sensing performance as well **[187]**. The cross-sectional view of TEM micrographs revealing thicknesses of 20 nm NiO/100 nm SnO$_2$ at low magnification (**Figure 17g**), and interface of the 20 nm NiO/100 nm SnO$_2$ at high magnification (**Figure 17h**). The formation of NiO/SnO$_2$ p-n heterojunction gas sensor is illustrated in **Figure 17i**. The gas sensing mechanism of NiO/SnO$_2$ p-n heterojunction gas sensor is also depicted in **Figure 17j**. Fang et al. **[188]** showed p-n heterostructure thin film that was made up of NiO deposited by electron beam evaporation and SnO$_2$ assembled by RF magnetron sputtering. These sensors revealed significantly improved ethanol vapour gas sensing characteristics. A superb response of 7.9 at working temperature of 250 ^{o}C for 100 ppm ethanol vapor was observed. Kumar et al. **[189]** reported a rapid response using the gas sensors fabricated from TiO$_2$ and NiO nanostructured bilayer thin films when tested to 5-500 ppm ammonia gas within low working temperature system (30 – 300 ^{o}C).

The TiO$_2$/NiO and NiO/TiO$_2$ sensors depicted a relatively high sensing responses (R$_g$/R$_a$ ~7.6) and (R$_a$/R$_g$ ~ 5.0) with extremely quick response times ~ 24 and 30 s towards 100 ppm NH$_3$ gas at 280 and 300 ^{o}C, respectively.
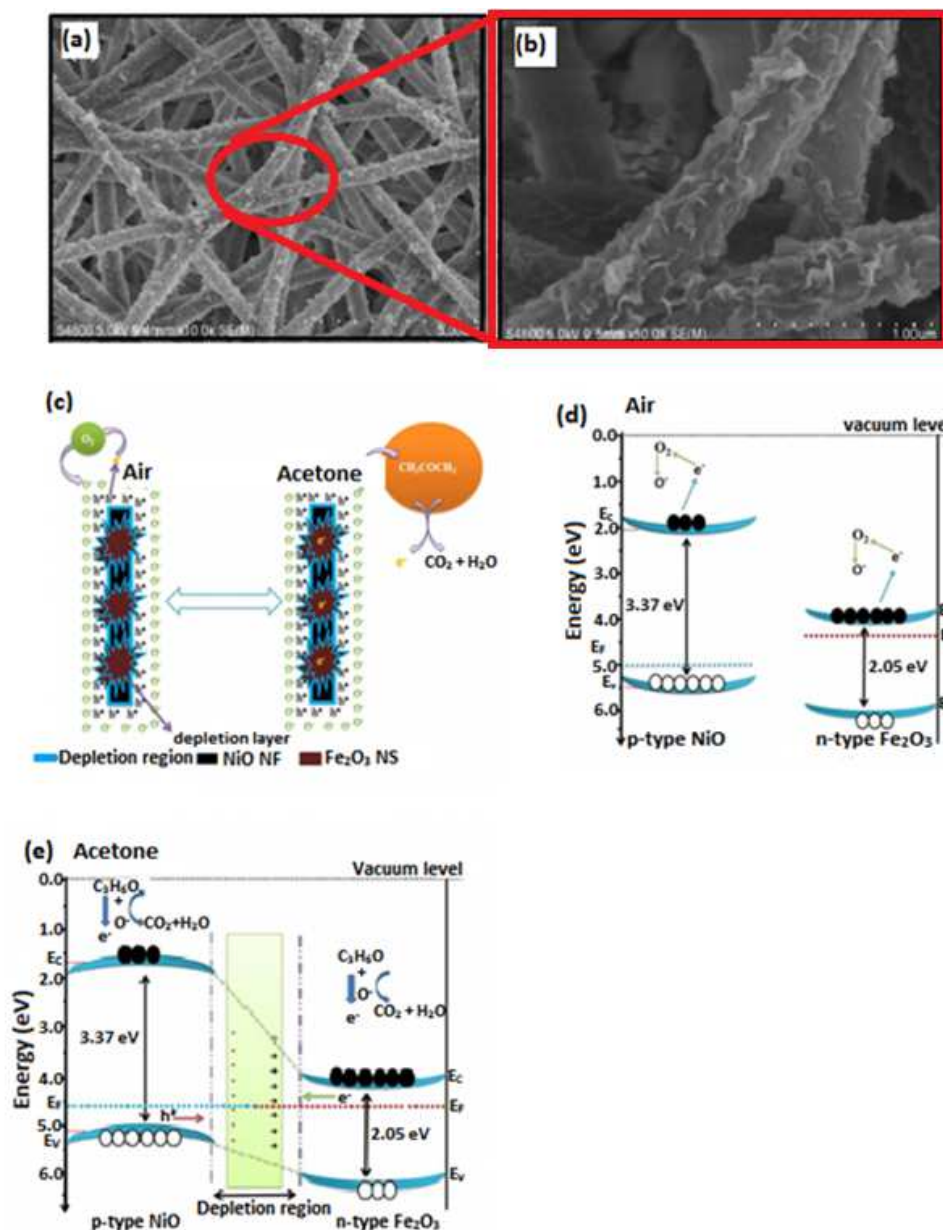
Figure 16: SEM micrographs of nanocomposites on Fe$_2$O$_3$/NiO fibers assembled by nanosheets (a) low and (b) high magnification. (c) Schematic diagrams of the acetone sensing mechanism of Fe$_2$O$_3$/NiO p-n heterostructure nanosheet-coverd fibers during the exposure of air and analyte gas acetone, and the recommended energy band structure of (d) pure NiO and Fe$_2$O$_3$ in air and (e) Fe$_2$O$_3$/NiO p-n heterojunction in acetone. (NF: nanofibers and NS: nanosheet). (Reprinted with permission from Ref. **[176]**. Copyright 2017: Elsevier)
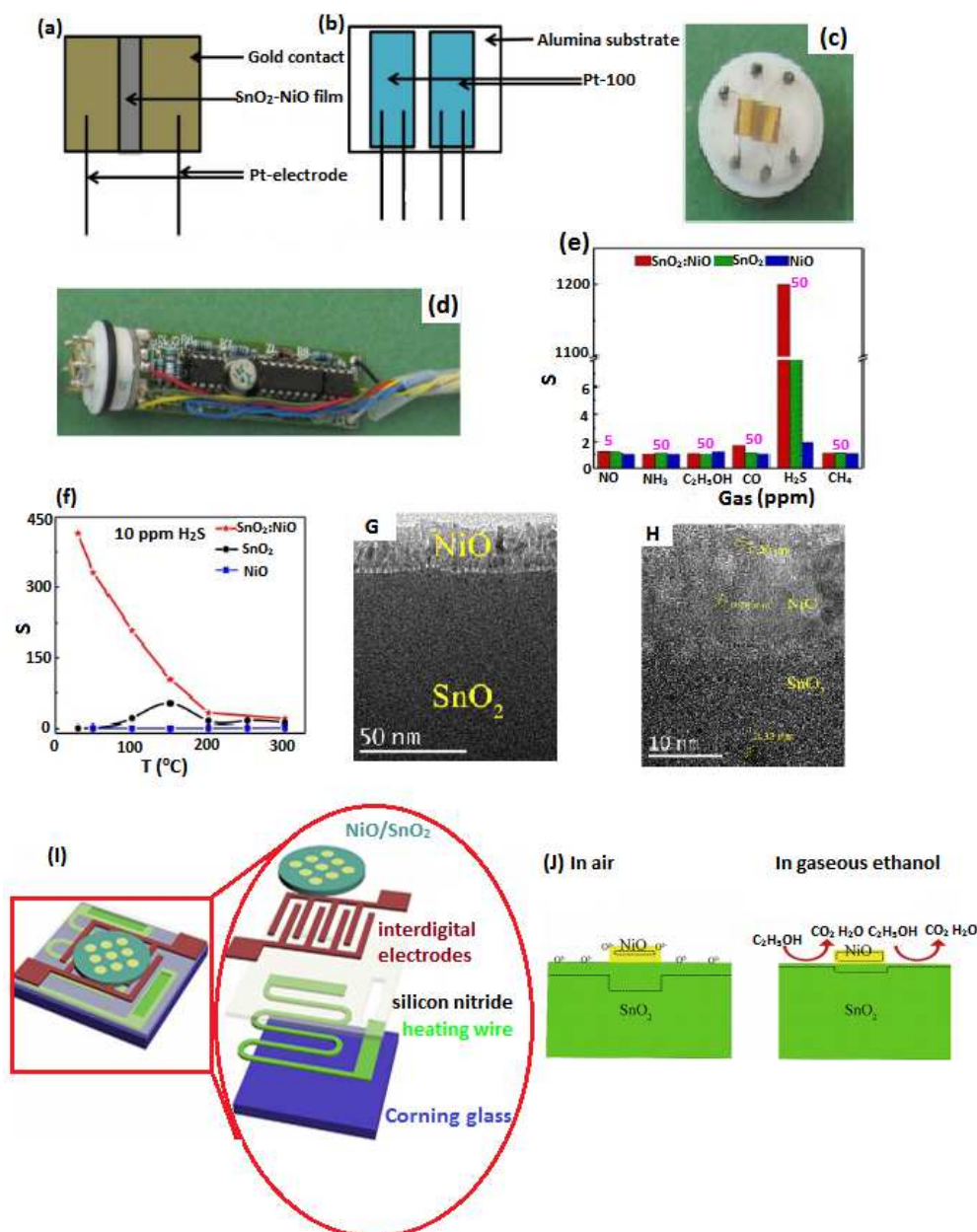
Figure 17: Schematic diagram of the sensor component (a) film side, (b) Pt-100s connected on the rear side of sensor component and real images of (c) sensor film on a Teflon head (d) sensor with Teflon head attached to a circuit with temperature controller. (e) Selectivity histogram of pure SnO_2, NiO and p-n SnO_2:NiO gas sensors towards various gases at room temperature. (f) Sensor response against operating temperature of pure SnO_2, NiO and p-n SnO_2:NiO gas sensors. (Reprinted with permission from Ref. **[186]**. Copyright 2017: Elsevier). Cross-sectional TEM micrograph: (g) 20 nm NiO/100 nm SnO_2 at low magnification, (h) interface of the 20 nm NiO/100 nm SnO_2 at high magnification. (i) The formation of NiO/SnO_2 heterojunction gas sensor. (j) Gas sensing mechanism of the NiO/SnO_2 sensor. (Reprinted with permission from Ref. **[188]**. Copyright 2017: Elsevier).

3D heterostructures can be assembled into low dimensional nano-building blocks, including 0D nanoparticles, 1D nanowires and 2D nanosheets as illustrated in **Figure 18a – f**. This special 3D heterostructures provide better performance compared with bulk nanomaterials, due to relative big internal capacity among the nanosheets which provides facile transport routes or channels making the diffusion of gas molecules more straightforwardly **[190]**. In addition, the morphologies of SMO with hierarchical heterostructures can be altered to improve the gas diffusion rate and enhance the specific surface area, and furthermore, intensify the gas sensing features **[191]**. In this section we briefly discussed critical recent development of NiO nanocomposite gas sensors with hierarchical morphology. Kim et al. **[192]** revealed that the NiO/NiMoO$_4$ based gas sensors hierarchical spheres possessed a maximum resistance ratio of 101.5 (big response) towards 5 ppm p-xylene gas with resistance ratios less than 30 (low cross responses) toward 5 ppm toluene, benzene, C$_2$H$_5$OH, CH$_3$COCH$_3$, HCHO, trimethylamine and NH$_3$ gases. The improvement in gas sensing performance towards xylene is due to the synergistic composite between NiO and NiMoO$_4$, gas-accessible hierarchical structure, and electronic sensitization by incorporation of Mo. Liu et al. **[193]** investigated the gas sensing performance of the flower-like NiO-decorated ZnO based sensor (see **Figure 18i**) towards various gases including formaldehyde, toluene, dimethylbenzene, methanol, ethanol and acetone as shown in **Figure 18g - h.** It was clearly seen that the 8 at.% NiO-decorated ZnO based gas sensor exhibited improved responses towards various analyte gases compared to its counterpart pure ZnO, showing higher response to acetone. The responses of sensors towards 100 ppm acetone gas were analysed precisely at different operating temperature in the range of 200 to 375 $^{\circ}$C to observe the optimum content of NiO and working temperature, as demonstrated in **Figure 18i**. The band

arrangement at the interface of the NiO/ZnO p-n nanoheterostructure is shown in schematic form in **Figure 18j**. Firstly, the composite of different MOX results to band bending, which initiates a potential barrier at the heterojunctions. The potential barrier obstructs the transmission of electron via the nanostructures, and therefore provides more electrons for extra oxygen molecules to adsorb on the surface of the sensing layer, which effectively enhances the sensor performance. Lastly, the creation of p-n heterojunction at the interface of various MOX possesses relative high energy and therefore can behave as the active site to catalyse the decomposition of analyte gas molecules **[194]**. The sensing mechanism with appropriate and excess amounts of NiO into the ZnO is illustrated in **Figure 18k**. While, the 3-D nanostructured based sensors appear to be promising contenders for gas sensing nanomaterials, however, it is very vital to enhance the device performances to serve a purpose of practical applications. The nanosized heterostructures of MOX have attracted much attention because they possess enhanced physical and chemical properties with respect to their single-component counterpart. **Table 4** depicts the comparison study of heterostructures of NiO with other n-type MOX and their gas sensing properties.
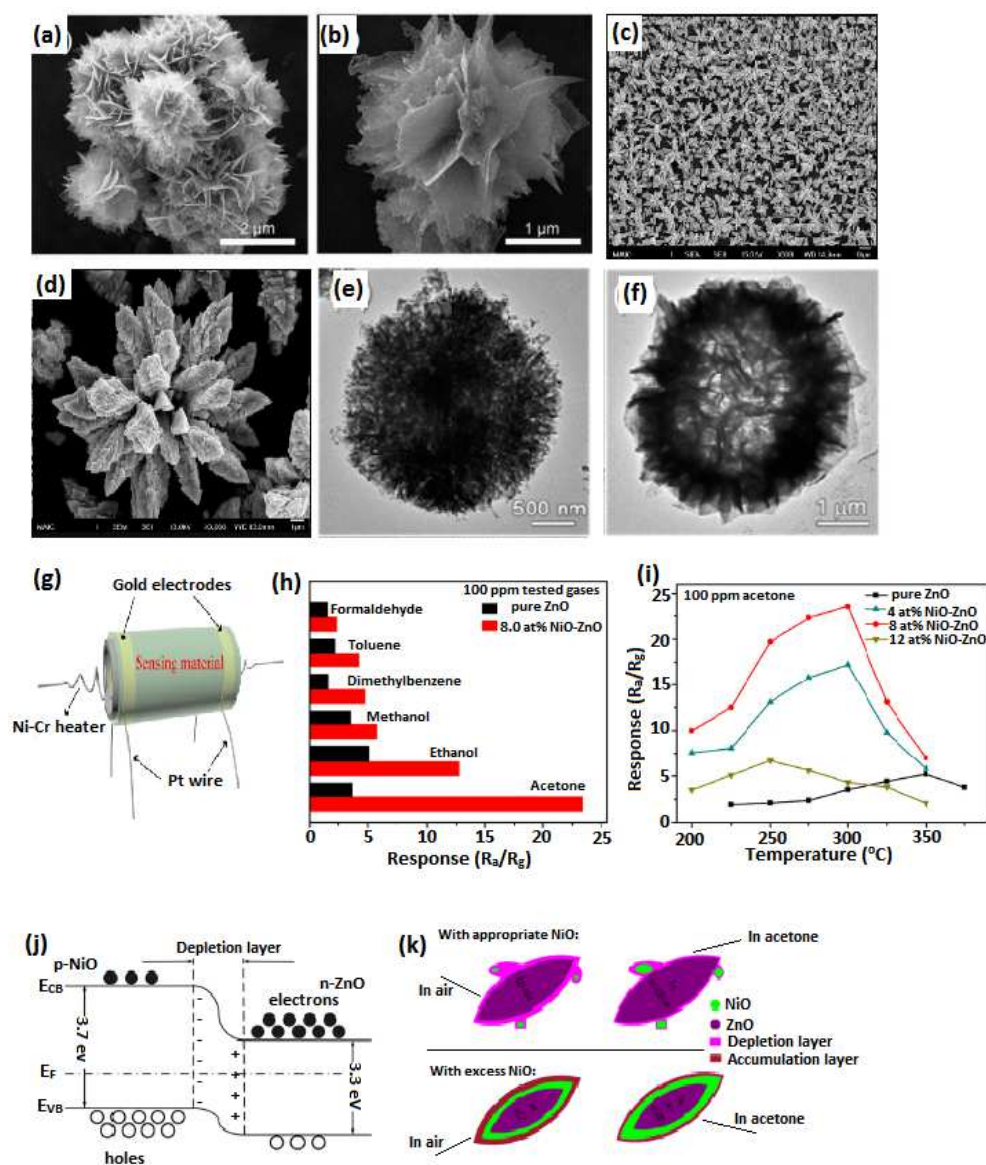
Figure 18: SEM micrographs of (a) and (b) 3-D SnO$_2$ flower-like microstructure. (Reprinted with permission from Ref. **[190]**. Copyright 2016: Elsevier). (c) Low and (d) high magnification of bismuth oxide flower-like. (Reprinted with permission from Ref. **[191]**. Copyright 2010: American Chemical Society). TEM images of (e) NiO and (f) NiO/NiMoO$_4$ nanocomposites. (Reprinted with permission from Ref. **[192]**. Copyright 2016: American Chemical Society). (g) Schematic diagram of a sensor. (h) The responses of pure ZnO and p-n ZnO/NiO sensors to different gases at 300 ^{o}C with similar concentration. (i) The responses of pure ZnO and p-n NiO/ZnO sensor with hierarchical flower-like morphology against operating temperature to 100 ppm acetone gas. (j) Schematic illustration of band arrangement of the p-n NiO/ZnO nanoheterostructure.(k) Sketch of gas sensing mechanism with various content of NiO. (Reprinted with permission from Ref. **[193]**. Copyright 2016: Elsevier).

Table 4: Comparison study of heterostructures of p-type NiO and other n-type MOX and their gas sensing properties.

Heterostructures	Morphology	Analyte gas	Gas concentration (ppm)	T_{op} (^{o}C)	Response	Refs.
NiO-ZnO	Flower-like	Acetone	200	300	38.8	[193]
NiO-SnO$_2$	Nanowebs	Ethanol	100	300	27.5	[172]
NiO-Fe$_2$O$_3$	Nanoplate	H$_2$S	200	300	26.55	[195]
NiO-TiO$_2$	Nanorods	Acetone	200	400	9.33	[168]
NiO-ZnO	Nanowire	H$_2$S	100	RT	31.5	[196]
NiO-Al$_2$O$_3$	Nanoparticles	2-Chloroethanol	20	160	6.8	[197]
NiO-SnO$_2$	Nanorods	Ethanol	50	320	94.8	[24]
NiO-RuO$_2$	Nanoparticles	Ethanol	2000	350	35.9	[25]
NiO-NiMoO$_4$	Hierarchical spheres	p-Xylene	5	375	105	[192]
NiO/ZnO	Hollow spheres	Acetone	100	275	29.8	[162]
NiO/ZnO	Nanoplates	Ethanol	800	400	40.72	[160]
NiO-rGO-SnO$_2$	Nanoplates	NO$_2$	60	RT	62.27	[198]
NiO@CuO	Nanosheets	NO$_2$	100	RT	78	[199]
PdO-NiO	Spherical	H$_2$S	20, 100	60	43, 95	[200]
NiO-Nb$_2$O$_5$	Nanoparticles	Hydrogen	500	RT	1.68	[163]
NiO-ZnO	Nanosheets	Acetone	100	240	205.15	[201]
NiO-SnO$_2$	Nanowires	NO$_2$	15	250	9.34	[202]
NiO-SnO$_2$	Microcubes	Formaldehyde	100	240	27	[53]
NiO-SnO$_2$	Nanoparticles	H$_2$S	10	RT	440	[186]
NiO-SnO$_2$	Nanoparticles	SO$_2$	500	180	56	[203]

NiO-SnO$_2$	Nanosheets	NO$_2$	0.5	85	20	**[204]**
NiO-SnO$_2$	Nanoparticles	Ethanol	100	250	7.9	**[188]**
NiO-In$_2$O$_3$	Nanofibers	Ethanol	100	300	78	**[177]**
NiO-rGO	Nanocube	H$_2$S	50	92	31.95	**[205]**
NiO-NiWO$_4$	Yolk-shell spheres	p-Xylene	5	350	343.5	**[165]**
NiO-ZnO	Nanowires	Ethanol	100	500	-	**[173]**
NiO-WO$_3$	Nanofibers	Acetone	100	375	22.5	**[175]**
NiO-ZnO	Microsphere	Ethanol	100	260	61	**[206]**
NiO-SnO$_2$	Flower-like	Acetone	50	300	20.18	**[207]**
NiO-Zn$_2$SnO$_4$-SnO$_2$	Porous hollow cube	Ethanol	100	280	52.7	**[208]**
NiO-ZnO	Microflowers	Ethanol	100	350	54	**[209]**
NiO-SnO$_2$	Nanoflower	Toluene	100	250	66.3	**[210]**
NiO-Fe$_2$O$_3$	Nanosheets	Ethanol	100	255	170.7	**[211]**
NiO-CuInS$_2$	Quantum dots	NO$_2$	30	RT	~ 7.5	**[212]**
NiO@ZnSnO$_3$	Microspheres	Formaldehyde	1	85	10.4	**[164]**
NiO-SnO$_2$	Nanowebs	NO$_2$	10	300	36	**[213]**
NiO-ZnO	Nanowires	Ethanol	50	400	6.7	**[214]**
		Acetone	100	400	10	
NiO@rGO	Nanosheets	Hydrogen	1	-	0.64	**[215]**
NiO-SnO$_2$	Microflowers	Formaldehyde	100	100	39.2	**[216]**
NiO-ZnO	Microflowers	Formaldehyde	100	200	26.2	**[217]**

NB. Hyphen "-"represents that the value is not reported. RT represents room temperature.

9. Conclusion and Remarks

The preparation of p-type NiO based gas sensors by various methods such as hydrothermal/solvothermal, sol-gel, chemical/co-precipitation and microemulsion were reviewed. Chemical/co-precipitation is a very reliable and low-cost method, however, it is very challenging to manipulate the particle and/or grain size and structural morphology due to the speedy precipitation, while the sol-gel method offers high compositions, high purity, low temperature and the control of the particle size and shape and hydrothermal or solvothermal is considered as a method that requires long synthesis to attain nucleation and growth of nanoparticles. On the brightest side, this synthesis method offers a relatively good control over homogeneity, chemical compositions, particle size, phase and morphology of the end products. It was further noticed that amongst the various synthesis methods, a substantial number of work related NiO based sensors has been carried out utilizing hydrothermal method. The microemulsion method is categorized into water-in-oil, oil-in-water and water-in-supercritical-CO_2. The influence of noble metals on NiO based gas sensors has been classified as chemical and/or electronic sensitization. This verified that the catalytic effects of these noble metals play a vital role in improving the NiO gas sensing characteristics. On the other side, the TM on MOX based gas sensors behaved as surface sites for adsorbates, catalyst or promoters for surface reaction and as elements stimulating enhancement in the thermal stability of nanostructured materials. The most used TMDs are MoS_2, $MoSe_2$, WS_2 and WSe_2 sensors. These TMDs consist of three atomic layers which are joined together by weak Van der Waals interaction, and this result in a reducing number of active sites. The increase in number of active sites is achieved by functionalizing these TMDs with conductive templates such as graphene or graphene oxide. The gas sensing

mechanism of TMDs is mainly dependent on charge transfer process. The improvement of sensing characteristics in phosphors material is due to rapidly oxygen ion mobility, effective catalytic nature and large surface basicity. The presence of more 4f electrons in phosphors is more ease for oxygen molecules to transform reactive oxygen species. The conducting polymers such as PPy, PANI, P3HT, PEDOT and PTh consist of π-bonds on their backbone, which assist in the movement of the electrons through the polymeric chain. These conducting polymers based gas sensors can be able to sense in relatively low operating temperature than some MOX based gas sensors.

Throughout the literature, it was noticed that 0D, 1D, 2D and 3D heterostructures on NiO have improved gas sensing properties drastically. In most cases, the improvement in sensing was due to various morphologies with relative large surface areas, which provided sufficient adsorption sites for all involved molecules in a small space. The creation of p-n heterojunction at the interface between p-type NiO and n-type MOX possessed relatively high energy and therefore can behave as the active site to catalyse the decomposition of analyte gas molecules. The synergistic effect between NiO and other MOX was also the contributing factors towards the better sensing mechanism. This review article revealed that limited work, especially in the field of TMDs/NiO, phosphors/NiO, and conducting polymers/NiO gas sensors has been done. Throughout the literature, there were no reports on MoS_2, $MoSe_2$ and WS_2/NiO based gas sensors. Again, we discovered that the studies on rare-earths/NiO gas sensors are very limited, most of the studies have focused on the Ce-NiO and CeO_2-NiO based sensors. The most studies on conducting polymers were done on PPy/NiO sensors; however, the studies on PANI and P3HT/NiO nanocomposite based sensors are also limited.

Therefore, the future work should strongly attempt to focus on the gas sensing characteristics of MoS_2/NiO, $MoSe_2/NiO$ and WS_2/NiO as well as rare-earths/NiO gas, particularly; the composite of MoS_2/NiO sensor will be designed and/or fabricated for humidity detection. Additionally, focus on the incorporation of P3HT polymer on the NiO and their gas sensing a low operating temperature should be considered. Regardless of all astonishing developments accomplished with heterostructured sensors, especially for NiO based sensors, likely diffusion through the junctions, reproducibility of the nanostructures, catalytic influences amongst the nanostructures creating the heterostructures and the stability between the two different nanomaterials need to be studied carefully. The concept of utilizing NiO to enhance the moisture-resistant of the SMO gas sensors is very imperative and should be considered very carefully as well, particularly in biological applications such as diabetes diagnosis. Besides, synthesis of both nanostructures in a controlled manner, especially for commercial devices is extremely vital. This may help to close the breach between the research and practical exploitation.

Acknowledgements

References

[1]   Y. Bao, P. Xu, S. Cai, H. Yu, X. Li, Detection of volatile-organic-compounds (VOCs) in solution using cantilever-based gas sensors, Talanta, 182 (2018) 148 – 155.

[2]   S. Yang, C. Jiang, S.-H. Wei, Gas sensing in 2D materials, Applied Physics Reviews, 4 (2017) 021304.

[3]   J.P. Cheng, J. Wamg, Q.Q. Li, H.G. Li, Y. Li, A review of recent developments in tin dioxide composites for gas sensing application, Journal of Industrial and Engineering Chemistry, 44 (2016) 1 – 22.

[4]   D. Ju, H. Xu, J. Zhang, J. Guo, B. Cao, Direct hydrothermal growth of ZnO nanosheets on electrode for ethanol sensing, Sensor and Actuators B, 201 (2014) 444 – 451.

[5]   L. Zhu, W. Zeng, Room-temperature gas sensing of ZnO based gas sensor: A review, Sensors and Actuators A, 267 (2017) 242 – 261.

[6]   R. Zhao, K. Li, Z. Wang, X. Xing, Y. Wang, Gas-sensing performances of Cd-doped ZnO nanoparticles synthesized by a surfactant-mediated method for n-butanol gas, Journal of Physics and Chemistry of Solids, 112 (2018) 43 – 49.

[7]   I. Kortidis, H.C. Swart, S.S. Ray, D.E. Motaung, Characteristics of point defects on the room temperature ferromagnetic and highly NO_2 selectivity gas sensing of p-type Mn_3O_4 nanorods, Sensors and Actuators B, 285 (2019) 92 – 107.

[8]   D.N. Oosthuizen, D.E. Motaung, H.C. Swart, Selective detection of CO at room temperature with CuO nanoplatelets sensor for indoor air quality monitoring manifested by crystallinity, Applied Surface Science, 466 (2019) 545 – 553.

[9]   Z. Hu, D. Chen, P. Yang, L. Yang, L. Qin, Y. Huang, X. Zhao, Sol-gel processed ytrrium doped NiO as hole transport layer in inverted perovskite solar cells for enhanced performance, Applied Surface Science, 441 (2018) 258 - 264.

[10]   Y. Yu, Y. Xia, W. Zeng, R. Liu, Synthesis of multiple networked NiO nanostructures for enhanced gas sensing performance, Materials Letters, 206 (2017) 80 – 83.

[11] Y. Zhang, W. Zeng, New insight into gas sensing performance of nanoneedle-assembled and nanosheet-assembled hierarchical NiO nanoflowers, Materials Letters, 195 (2017) 217 – 219.

[12] J.P. Kumar, S.D. Giri, A. Sarkar, Mesoporous NiO with different morphology: Synthesis, characterization and their evaluation for oxygen evolution reaction, International Journal of Hydrogen Energy, 43 (2018) 15639 - 15649.

[13] H. W. Kim, S.-W. Choi, A. Katoch, S.S. Kim, Enhanced sensing performances of networked SnO_2 nanowires by surface modification with atmospheric pressure Ar – O_2 plasma, Sensors and Actuators B, 177 (2013) 654 – 658.

[14] Y. Lu, Y.H Ma, S.Y Ma, W.X Jin, S.H Yan, X.L Xu, Q. Chen, Curly porous NiO nanosheets with enhanced gas-sensing properties, Materials Letters, 190 (2017) 252 – 255.

[15] R. Miao, W. Zeng, Q. Gao, SDS-assisted hydrothermal synthesis of NiO flake-flower architectures with enhanced gas-sensing properties, Applied Surface Science, 384 (2016) 304 – 310.

[16] Kwon-Il Choi, M. Hubner, A Haensch, H.-J. Kim, U. Weimar, N. Barsan, J.-H. Lee, Ambivalent effect of Ni loading on gas sensing performance in SnO_2 based gas sensor, Sensors and Actuators B 183 (2013) 401– 410.

[17] Microstructure, electrical and humidity sensor properties ofelectrospun NiO–SnO2nanofibersPetronela Pascariua,∗, Anton Airineia, Niculae Olarua, Iulian Petrilab,c, Valentin Nicad,Liviu Sacarescua, Florin TudoracheSensors and Actuators B 222 (2016) 1024–1031

[18] A. Mirzaei, G. Neri, Microwave-assisted synthesis of metal oxide nanostructures for gas sensing application: A review, Sensors and Actuators B, 237 (2016) 749 – 775.

[19] R.S. Kate, S.A. Khalate, R.J. Deokate, Overview of nanostructured metal oxides and pure NiO electrodes for supercapacitors: A review, Journal of Alloys and Compounds, 734 (2018) 89 – 111.

66

[20]   W. Xing, F. Li, Z.-F. Yan, G.Q. Lu, Synthesis and electrochemical properties of mesoporous nickel oxide, Journal of Power Sources, 134 (2004) 324 – 330.

[21] R. Krishnakanth, G. Jayakumar, A.A. Irudayaraj, A.D. Raj, Structural and magnetic properties of NiO and Fe-doped NiO nanoparticles synthesized by chemical co-precipitation method, Materials Today: Proceedings, 3 (2016) 1370 – 1377.

[22]   R.L. Fomekong, H.M.T. Kamta, J.N. Lambi, D. Lahem, A sub-ppm level formaldehyde gas sensor based on Zn-doped NiO prepared by a co-precipitation route, Journal of Alloys and Compounds, 731 (2018) 1188 – 1196.

[23]   F. Yang, Z. Guo, Engineering NiO sensitive materials and its ultra-selective detection of benzaldehyde, Journal of Colloid and Interface Science, 467 (2016) 192 – 202.

[24]   G. Sun, H. Chen, Y. Li, Z. Chen, S. Zhang, G. Ma, T. Jia, J. Cao, H. Bala, X. Wang, Z. Zhang, Synthesis and improved gas sensing properties of NiO decorated SnO_2 microflowers assembled with porous nanorods, Sensors and Actuators B, 233 (2016) 180 – 192.

[25]   V. Kruefu, A. Wisitsoraat, D. Phokharatkul, A. Tuantranont, S. Phanichphant, Enhancement of p-type gas-sensing performances of NiO nanoparticles prepared by precipitation with RuO_2 impregnation, Sensors and Actuators B, 236 (2016) 466 – 473.

[26]   A. Kitai, Luminescent Materials and Applications, (2008), John Wiley & Sons, page 40.

[27]   L.L. Hench, J.K. West, The sol gel process, Chemical Reviews, 90 (1990) 33 – 72.

[28]   S. Park, C.-H. Kim, W.-J. Lee, S.Sung, M.-H. Yoon, Sol-gel metal oxide dielectrics for all-solution processed electronics, Materials Science and Engineering R, 114 (2017) 1 – 22.

[29]   M.R. Mohammadi, Semiconductor TiO_2-Al_2O_3 thin film gas sensors derived from aqueous particulate sol-gel process, Materials Science in Semiconductor Processing, 27 (2014) 711 – 718.

[30] S. Zhao, Y. Shen, P. Zhou, J. Zhang, W. Zhang, X. Chen, D. Wei, P. Fang, Y. Shen, Highly selective NO_2 sensor based on p-type nanocrystalline NiO thin films prepared by sol-gel dip coating, Ceramics International, 44 (2018) 753 – 759.

[31] I. Sta, M. Jlassi, M. Kandyla, M. Hajji, P. Koralli, R. Allagui, M. Kompitsas, H. Ezzaouia, Hydrogen sensing by sol-gel grown NiO and NiO:Li thin films, Journal of Alloys and Compounds, 626 (2015) 87 – 92.

[32] S.R. Gawali, V.I. Patil, V.G. Deonikar, S.S. Patil, D.R. Patil, P.S. Patil, J. Pant, Ce doped NiO nanoparticles as selective NO_2 gas sensor, Journal of Physics and Chemistry of Solids, 114 (2018) 28 – 35.

[33] N.K.V. Nadimpalli, R. Bandyopadhyaya, V. Runkana, Thermodynamic analysis of hydrothermal synthesis of nanoparticles, Fluid Phase Equilibria, 456 (2018) 33 – 45.

[34] J. Shi, J. Sun, B. Fang, Q. Du, S. Zhang, J. Ding, Photoluminescence performance of Er/Yb co-doped NBT ceramics prepared via hydrothermal method, Journal of Physics and Chemistry of Solids, 121 (2018) 228 – 235.

[35] H. Wang, W. Song, M. Zhang, Q. Zhen, M. Guo, Y. Zhang, X. Du, Hydrothermally grown and self-assembled modified titanium and nickel oxide composite nanosheets on Nitinol-based fibers for efficient solid phase microextraction, Journal of Chromatography A, 1468 (2016) 33 - 41.

[36] Y. Yu, Y. Xia, W. Zeng, R. Liu, Synthesis of multiple networked NiO nanostructures for enhanced gas sensing performance, Materials Letters, 206 (2017) 80 – 83.

[37] C. Kuang, W. Zeng, H. Ye, Y. Li, A novel approach for fabricating NiO hollow spheres for gas sensors, Physica E: Low-dimensional Systems and Nanostructures, 97 (2018) 314 – 316.

[38] Z. Li, Supersensitive and superselective formaldehyde gas sensor based on NiO nanowires, Vacuum, 143 (2017) 50 – 53.

[39] F. Yan, J. Texter, Capturing nanoscopic length scales and structures by polymerization in microemulsions, Soft Matter, 2 (2006) 109 – 118.

[40] A.K. Ganguli, A. Ganguly, S. Vaidya, Microemulsion-based synthesis of nanocrystalline materials, Chemical Society Reviews, 39 (2010) 474 – 485.

[41] A. Salabat, F. Mirhoseini, A novel and simple microemulsion method for synthesis of biocompatible functionalized gold nanoparticles, Journal of Molecular Liquids, 268 (2018) 849 – 853.

[42] M. Schwarze, T. Pogrzeba, I. Volovych, R. Schomacker, Microemulsion systems for catalytic reactions and processes, Catalysis Science & Technology, 5 (2015) 24 -33.

[43] J.P. Wilcoxon, B.L. Abrams, Synthesis, structure and properties of metal nanoclusters, Chemical Society Reviews, 35 (2006) 1162 - 1194.

[44] Y. Du, W. Wang, X. Li, J. Zhao, J. Ma, Y. Liu, G. Lu, Preparation of NiO nanoparticles in microemulsion and its gas sensing performance, Materials Letters, 68 (2012) 168 – 170.

[45] Y. Wang, Q. Su, Synthesis of NiO/Ag nanocomposites by microemulsion method and the capacitance performance as electrodes, Journal of Materials Science: Materials in Electronics, 27 (2016) 4752 – 4759.

[46] M. Patel, J.S. Kim, B.S. Kim, J. Kim, Optical and photoelectrochemical properties of transparent NiO quantum dots, Materials Letters, 218 (2018) 123 - 126.

[47] N.D. Hoa, C.M. Hung, N.V. Duy, N.V. Hieu, Nanoporous and crystal evolution in nickel oxide nanosheets for enhanced gas-sensing performance, Sensors and Actuators B, 273 (2018) 784 – 793.

[48] A.A. Khaleed, A. Bello, J.K. Dangbegnon, D.Y. Momodu, M.J. Madito, F.U. Ugbo, A.A. Akande, B.P. Dhonge, F. Barzegar, O. Olaniyan, B.W. Mwakikunga, Effect of activated carbon on the enhancement of CO sensing performance of NiO, Journal of Alloys and Compounds, 694 (2017) 155 – 162.

[49] K. Tian, X.-X. Wang, H.-Y. Li, R. Nadimicherla, X. Guo, Lotus pollen derived 3-dimensional hierarchically porous NiO microspheres for NO_2 gas sensing, Sensors and Actuators B, 227 (2016) 554 – 560.

[50] L. Lin, T. Liu, B. Miao, W. Zeng, Hydrothermal fabrication of uniform hexagonal NiO nanosheets: Structure, growth and response, Materials Letters, 102 (2013) 43 – 46.

[51] R. Miao, W. Zeng, Hydrothermal synthesis of flake-flower NiO architectures: Structure, growth and gas-sensing properties, Materials Letters, 171 (2016) 200 – 203.

[52] R. Miao, W. Zeng, Q. Gao, Hydrothermal synthesis of novel NiO nanoflowers assisted with CTAB and SDS respectively and their gas-sensing properties, Materials Letters, 186 (2017) 175 – 177.

[53] C. Gu, Y. Cui, L. Wang, E. Sheng, J.-J. Shim, J. Huang, Synthesis of the porous NiO/SnO_2 microspheres and microcubes and their enhanced formaldehyde gas sensing performance, Sensors and Actuators B, 241 (2017) 298 – 307.

[54] A.M. Soleimanpour, A.H. Jayatissa, G. Sumanasekera, Surface and gas sensing properties of nanocrystalline nickel oxide thin films, Applied Surface Science, 276 (2013) 291 – 297.

[55] Q. Du, L. Wang, J. Yang, J. Liu, Y. Yuan, M. Wang, B. Liu, X. Zhang, Y. Ren, H. Zhao, H. Yang, Enhancing gas sensing performances and sensing mechanism at atomic and molecule level of WO_3 nanoparticles by hydrogenation, Sensors and Actuators B, 273 (2018) 1786 - 1793.

[56] A. Oprea, N. Barsan, U. Weimar, Characterization of granular metal oxide semiconductor gas sensitive layers by using Hall effect based approaches, Journal of Physics D: Applied. Physics, 40 (2007) 7217 – 7237.

[57] G. Khorshidi, M. Behzad, H.M. Jahromi, E. Alaie, Influence of metal (W, Pd)-doping on gas sensing properties of the NiO flower-like thin films for o-xylene detection, Journal of Alloys and Compounds, 737 (2018) 122 – 129.

[58] C. Feng, C. Wang, H. Zhang, X. Li, C. Wang, P. Cheng, J. Ma, P. Sun, Y. Gao, H. Zhang, Y. Sun, J. Zheng, G. Lu, Enhanced sensitive and selective sensors using W – doped NiO nanotubes, Sensors and Actuators B, 221 (2015) 1475 – 1482.

70

[59] D. Abubakar, N.M. Ahmed, S. Mahmud, N.A. Algadri, Properties of NiO nanostructured growth using thermal dry oxidation of nickel metal thin film for hydrogen gas sensing at room temperature, Materials Research Express, 4 (2017) 075009 – 075020.

[60] X. Deng, L. Zhang, J. Guo, Q. Chen, J. Ma, ZnO enhanced NiO-based gas sensors towards ethanol, Materials Research Bulletin, 90 (2017) 170 – 174.

[61] S.U. Mutkule, S.T. Navale, V.V. Jadhav, S.B. Ambade, M. Naushad, A.D. Sagar, V.B. Patil, F.J. Stadler, R.S. Mane, Solution-processed nickel oxide films and their liquefied petroleum gas sensing activity, Journal of Alloys and Compounds, 695 (2017) 2008 – 2015.

[62] S.T. Navale, V.V. Jadhav, K.K. Tehare, R.U.R. Sagar, C.S. Biswas, M. Galluzzi, W. Liang, V.B. Patil, R.S. Mane, F.J. Stadler, Solid-state synthesis strategy of ZnO nanoparticles for the rapid detection of hazardous Cl_2, Sensors and Actuators B, 238 (2017) 1102 – 1110.

[63] Z.P. Tshabalala, D.E Motaung, G.H. Mhlongo, O.M. Ntwaeaborwa, Room temperature gas sensing characteristics of titanium dioxide nanostructures: Effects of hydrochloric acid on the structure and magnetic properties, MSc Thesis, (2016), University of the Free State, Bloemfontein, South Africa.

[64] D.R. Miller, S.A. Akbar, P.A. Morris, Nanoscale metal oxide-based heterojunctions for gas sensing: a review, Sensors and Actuators B, 204 (2014) 250 – 272.

[65] Y. Unutulmazsoy, R. Merkle, J. Mannhart, J. Maier, Chemical diffusion coefficient of Ni in undoped and Cr-doped NiO, Solid State Ionics, 309 (2017) 110 – 117.

[66] J. Zhang, D. Zeng, Q. Zhu, J. Wu, K. Xu, T. Liao, G. Zhang, C. Xie, Effect of grain boundaries in NiO nanosheet layers room temperature sensing mechanism under NO_2, The Journal of Physical Chemistry C, 119 (2015) 17930 – 17939.

[67] M. Wang, Y. Wang, J. Liu, C. Pei, B. Liu, Y.Yuan, H.Zhao, S. Liu, H. Yang, Enhanced sensing performance and sensing mechanism of hydrogenated NiO particles, Sensors and Actuators B, 250 (2017) 208 – 214.

[68]   D.N. Oosthuizen, D.E. Motaung, H.C. Swart, In depth study on the notable room-temperature NO_2 gas sensor based on CuO nanoplatelets prepared by sonochemical method: Comparison of various bases, Sensors and Actuators B, 266 (2018) 761 – 772.

[69]   D. Schonauer, T. Nieder, K. Wiesner, M. Fleischer, R. Moos, Investigation of the electrode effects in mixed potential type ammonia exhaust gas sensors, Solid State Ionics, 192 (2011) 38 – 41.

[70]   D. Schonauer, T. Nieder, K. Wiesner, M. Fleischer, R. Moos, Selective mixed potential ammonia exhaust gas sensor, Sensors and Actuators B, 140 (2009) 585 – 590.

[71]   Y. Wang, B. Liu, S. Xiao, X. Wang, L. Sun, Q. Li, Q. Zhang, T. Wang, Low temperature H_2S detection with hierarchical Cr-doped WO_3 microspheres, ACS Applied Materials & Interface, 8 (2016) 9674 – 9683.

[72]   M. Hubner, C.E. Simion, A. Haensch, N. Barsan, U. Weimar, CO sensing mechanism with WO_3 based gas sensors, Sensors and Actuators, 151 (2010) 103 – 106.

[73]   M. Hubner, C.E. Simion, A. Tomescu-Stanoiu, S. Pokhrel, N. Barsan, U. Weimar, Influence of humidity on CO sensing with p-type CuO thick film gas sensors, Sensors and Actuators B, 153 (2011) 347 – 353.

[74]   N.K. Singh, S. Shrivastava, S. Rath, S. Annapoorni, Optical and room temperature sensing properties of highly oxygen deficient flower-like ZnO nanostructures, Applied Surface Science, 257 (2010) 1544 – 1549.

[75]   Z.U. Abideen, J.-H.Kim, A. Mirzaei, H.W. Kim, S.S. Kim, Sensing behaviour to ppm level gases and synergistic sensing mechanism in metal-functionalized rGO-loaded ZnO nanofibers, Sensors and Actuators B, 255 (2018) 1884 – 1896.

[76]   A. Mirzaei, Jae-Hun Kim, Hyoun Woo Kim and Sang Sub Kim, How shell thickness can affect the gas sensing properties of nanostructured materials: Survey of literature, Sensors and Actuators B, 258 (2018) 270 – 294.

[77]   N. Yamazoe, G. Sakai, K. Shimanoe, Oxide semiconductor gas sensors, Catalysis Surveys from Asia, 7 (2003) 63 – 75.

[78]   Q. Xu, Z. Zhang, X. Song, S. Yuan, Z. Qiu, H. Xu, B. Cao, Improving the trimethylamine sensing performance based on debye length: A case study on α-Fe_2O_3@NiO(CuO) core-shell nanorods sensor working at near room temperature, Sensors and Actuators B, 245 (2017) 375 – 385.

[79]   A. Dey, Semiconductor metal oxide gas sensors: A review, Materials Science and Engineering: B, 229 (2018) 206 – 217.

[80]   G. Korotcenkov, Handbook of Gas Sensor Materials: Properties, Advantages and Shortcomings for Applications, Springer New York (2013) 275.

[81]   T.K. Pathak, H.C. Swart, R.E. Kroon, Structural and plasmonic properties of noble metal doped ZnO nanomaterials, Physica B: Condensed Matter, 535 (2018) 114 – 118.

[82]   T. Ishihara, K. Kometani, Y. Mizuhara, Y. Takita, Mixed oxide capacitor of CuO-$BaTiO_3$ as new type CO_2 gas sensor, Journal of the American Ceramic Society, 75 (1992) 613 – 618.

[83]   P. Rai, J.-W. Yoon, C.-H. Kwak, J.-H. Lee, Role of Pd nanoparticles in gas sensing behaviour of Pd@In_2O_3 yolk-shell nanoreactors, Journal of Materials Chemistry A, 4 (2016) 264 – 269.

[84]   J. Zhang, X. Liu, S. Wu, M. Xu, X. Guo, S. Wang, Au nanoparticle-decorated porous SnO_2 hollow spheres: a new model for a chemical sensor, Journal of Materials Chemistry, 20 (2010) 6453 – 6459.

[85]   M. Penza, C. Martucci, G. Cassano, NOx gas sensing characteristics of WO_3 thin films activated by noble metals (Pd, Pt, Au) layers, Sensors and Actuators B, 50 (1998) 52 – 59.

[86]   A. Cabot, J. Arbiol, J.R. Morante, U. Weimar, N. Barsan, W. Gopel, Analysis of the noble metal catalytic additives introduced by impregnation of as obtained SnO_2 sol gel nanocrystals for gas sensors, Sensors and Actuators B, 70 (2000) 87 – 100.

[87] Y. Luo, C. Zhang, B. Zheng, X. Geng, M. Debliquy, Hydrogen sensors based on noble metal doped metal oxide semiconductor: A review, International Journal of Hydrogen Energy, 42 (2017) 20386 – 20397.

[88] L. Wang, Z. Lou, T. Fei, T. Zhang, Enhanced acetone sensing performances of hierarchical hollow Au-loaded NiO hybrid structures, Sensors and Actuators B, 161 (2012) 178 – 183.

[89] P.V. Tong, N.D. Hoa, N.V. Duy, V.V. Quang, N.T. Lam, N.V. Hieu, In-situ decoration of Pd nanocrystals on crystalline mesoporous NiO nanosheets for effective hydrogen gas sensors, International Journal of Hydrogen Energy, 38 (2013) 12090 – 12100.

[90] J. Fu, C. Zhao, J. Zhang, Y. Peng, E. Xie, Enhanced gas sensing performance of electrospun Pt-functionalized NiO nanotubes with chemical and electronic sensitization, ACS Applied Materials & Interfaces, 5 (2013) 7410 – 7416.

[91] X. Gao, Z. Guo, Biomimetic superhydrophobic surfaces with transition metals and their oxides: A review, Journal of Bionic Engineering, 14 (2017) 401 – 439.

[92] N.D. Tho, D.V. Huong, H. T. Giang, P.Q. Ngan, G.H. Thai, D.T.A. Thu, D.T. Thu, N.T.M. Tuoi, N.N. Toan, P.D. Thang, H.N. Nhat, High temperature calcination for analysing influence of 3d transition metals on gas sensing performance of mixed potential sensor Pt/YSZ/LaMO$_3$ (M = Mn, Fe, Co, Ni), Electrochimica Acta, 190 (2016) 215 – 220.

[93] J.-W. Yoon, H.-J. Kim, I.-D. Kim, J.-H. Lee, Electronic sensitization of the response to C$_2$H$_5$OH of p-type NiO nanofibers by Fe doping, Nanotechnology, 24 (2013) 444005.

[94] X. Li, J.-F. Tan, Y.-E. Hu, X.-T. Huang, Microwave-assisted synthesis of Fe-doped NiO nanofoams assembled by porous nanosheets for fast response and recovery gas sensors, Material Research Express, 4 (2017) 045015 – 045026.

[95] X. Sun, X. Hu, Y. Wang, R. Xiong, X. Li, J. Liu, H. Ji, X. Li, S. Cai, C. Zheng, Enhanced gas-sensing performance of Fe-doped ordered mesoporous NiO with long-range periodicity, Journal of Physical Chemistry C, 119 (2015) 3228 – 3237.

[96]   L.R. Fomekong, D. Lahem, M. Debliquy, V. Dupont, L.J. Ngolui, A. Delcorte, Co-precipitation synthesis by malonate route, structural characterization and gas sensing properties of Zn-doped NiO, Materials Today: Proceedings, 3 (2016) 586 – 591.

[97]   C. Wang, X. Cui, J. Liu, X. Zhou, X. Cheng, P. Sun, X. Hu, X. Li, J. Zheng, G. Lu, Design of superior ethanol gas sensor based on Al-doped NiO nanorod flowers, ACS Sensors, 1 (2016) 131 – 136.

[98]   C. Feng, X. Kou, B. Chen, G. Qian, Y. Sun, G. Lu, One pot synthesis of In doped NiO nanofibers and their gas sensing properties, Sensors and Actuators B, 253 (2017) 584 – 591.

[99]   H.Gao, D. Wei, P. Lin, C. Liu, P. Sun, K. Shimanoe, N. Yamazoe, G. Lu, The design of excellent xylene gas sensor using Sn-doped NiO hierarchical nanostructure, Sensors and Actuators B, 253 (2017) 1152 – 1162.

[100]   T. Kamal, High performance NiO decorated graphene as a potential H_2 gas sensor, Journal of Alloys and Compounds, 729 (2017) 1058 – 1063.

[101]   C. Feng, X. Kou, X. Liao, Y. Sun, G. Lu, One-dimensional Cr-doped NiO nanostructures serving as a highly sensitive gas sensor for trace xylene detection, Royal Society of Chemistry Advances, 7 (2017) 41105 – 41110.

[102]   S. Bai, H. Fu, X. Shu, R. Luo, A. Chen, D. Li, C.C. Liu, NiO hierarchical hollow microspheres doped Fe to enhance triethylamine sensing properties, Materials Letters, 210 (2018) 305 – 308.

[103]   H.-I. Chen, C.-Y. Hsiao, W.-C. Chen, C.-H. Chang, T.-C. Chou, I.-P. Liu, K.-W. Lin, W.-C. Liu, Characteristics of a Pt/NiO thin film based ammonia gas sensor, Sensors and Actuators B, 256 (2018) 962 – 967.

[104]   S.M. Majhi, G.K. Naik, H.-J. Lee, H.-G. Song, C-R. Lee, I.-H. Lee, Y.-T. Yu, Au@NiO core-shell nanoparticles as a p-type gas sensor: Novel synthesis, characterization, and their gas sensing properties with sensing mechanism, Sensors and Actuators B, 268 (2018) 223 – 231.

[105] B.-Y. Kim, J.-W. Yoon, J.K. Kim, Y.C. Kang, J.-H. Lee, Dual role of multiroom-structured Sn-doped NiO microspheres for ultrasensitive and highly selective detection of xylene, ACS Applied Materials & Interfaces, 10 (2018) 16605 – 16612.

[106] J. Wei, X. Li, Y. Han, J. Xu, H. Jin, D. Jin, X. Peng, B. Hong, J. Li, Y. Yang, H. Ge, X. Wang, Highly improved ethanol gas sensing performance of mesoporous nickel oxides nanowires with the stannum donor doping, Nanotechnology, 29 (2018) 245501 – 245510.

[107] Y.-H. Wang, K.-J. Huang, X. Wu, Recent advances in transition-metal dichalcogenides based electrochemical biosensors: A review, Biosensors and Bioelectronics, 97 (2017) 306 – 316.

[108] M. Samadi, N. Sarikhani, M. Zirak, H. Zhang, H.-L. Zhang, A.Z. Moshfegh, Group 6 transition metal dichalcogenide nanomaterials: synthesis, applications and future perspectives, Nanoscale Horizons, 3 (2018) 90 – 204.

[109] D. Zhang, Y. Sun, P. Li, Y. Zhang, Facile Fabrication of MoS_2-modified SnO_2 hybrid nanocomposite for ultrasensitive humidity sensing, ACS Applied Materials Interfaces, 8 (2016) 14142 – 14149.

[110] D. Zhang, H. Chang, Y. Sun, C. Jiang, Y. Yao, J.W. Wang, Y. Song, Y.Q. Liang, X.M. Zhang, Fabrication of platinum-loaded cobalt oxide/molybdenum disulphide nanocomposite toward methane gas at low temperature, Sensors and Actuators B, 252 (2017) 624 – 632.

[111] D. Zhang, C. Jiang, J. Wu, Layer-by-layer assembled indium oxide nanocubes/flower-like molybdenum disulphide nanofilm for room temperature formaldehyde sensing, Sensors and Actuators B, 273 (2018) 176 – 184.

[112] X. Zhang, H. Zou, J. Peng, Z. Duan, M. Ma, X. Xin, W. Li, X. Zheng, Enhanced humidity sensing properties of $SmFeO_3$-modified MoS_2 nanocomposites based on the synergistic effect, Sensors and Actuators B, 272 (2018) 459 – 467.

[113] L. Ze, G. Yueqiu, L. Xujun, Z. Yong, MoS_2-modified ZnO quantum dots nanocomposite: Synthesis and ultrafast humidity response, Applied Surface Science, 399 (2017) 330 - 336.

[114] A. Venkatesan, S. Rathi, I.-Y. Lee, J. Park, D. Lim, M. Kang, H.-I. Joh, G.-H. Kim, E.S. Kannan, Molybdenum disulphide nanoparticles decorated reduced graphene oxide: highly sensitive and selective hydrogen sensor, Nanotechnology, 28 (2017) 365501.

[115] B. Cho, J. Yoon, S.K. Lim, A.R. Kim, D.H. Kim, S.-G. Park, J.-D. Kwon, Y.-J. Lee, K.-H. Lee, B.H. Lee, H.C. Ko, M.G. Hahm, Chemical sensing of 2D graphene/MoS_2 heterostructure device, ACS Applied Materals & Interfaces, 7 (2015) 16775 – 16788.

[116] A.S. Pawbake, R.G. Waykar, D.J. Late, S.R. Jadkar, Highly transparent wafer-scale synthesis of crystalline WS_2 nanoparticle thin film for photodetector and humidity-sensing applications, ACS Applied Materials & Interfaces, 8 (2016) 3359 – 3365.

[117] F. Perrozzi, S.M. Emamjomeh, V. Paolucci, G. Taglieri, L. Ottaviano, C. Cantalin, Thermal stability of WS_2 flakes and gas sensing properties of WS_2/WO_3 composite to H_2, NH_3 and NO_2, Sensors and Actuators B, 243 (2017) 812 – 822.

[118] D. Zhang, Y. Cao, P. Li, J. Wu, X. Zong, Humidity-sensing performance of layer-by-layer self-assembled tungsten disulphide/tin dioxide nanocomposite, Sensors and Actuators B, 265 (2018) 529 – 538.

[119] X. Li, X. Li, Z. Li, J. Wang, J. Zhang, WS_2 nanoflakes based selective ammonia sensors at room temperature, Sensors and Actuators B, 240 (2017) 273 – 277.

[120] K.Y. Ko, J.-G. Song, Y. Kim, T. Choi, S. Shin, C.W. Lee, K. Lee, J. Koo, H. Lee, J. Kim, T. Lee, J. Park, H. Kim, Improvement of gas-sensing performance of large-area tungsten disulphide nanosheets by surface functionalization, ACS Nano, 10 (2016) 9287 – 9296.

[121] L. Liu, L. Chen, G. Liu, A.N. Abbas, M. Fathi, C.W. Zhon, High performance chemical sensing using schottky-contacted chemical vapour deposition grown monolayer MoS_2 transistors, ACS Nano, 8 (2014) 5304 – 5314.

[122] W. Yang, L. Gan, H. Li, T. Zhai, Two-dimensional layered nanomaterials for gas-sensing applications, Inorganic Chemistry Frontiers, 3 (2016) 433.

[123] W. Yan, M.A. Worsley, T. Pham, A. Zettl, C. Carraro, R. Maboudian, Effects of ambient humidity and temperature on the NO_2 sensing characteristics of WS_2/graphene aerogel, Applied Surface Science, 450 (2018) 372 – 379.

[124] T. Xu, Y. Liu, Y. Pei, Y. Chen, Z. Jiang, Z. Shi, J. Xu, D. Wu, Y. Tian, X. Li, The ultra-high NO_2 response of ultra-thin WS_2 nanosheets synthesized by hydrothermal and calcination, Sensors and Actuators B, 259 (2018) 789 – 796.

[125] S. Fardindoost, S. Hatamie, A.I. Zad, F.R. Astaraei, Hydrogen sensing properties of nanocomposite graphene oxide/Co-based metal organic frameworks (Co-MOFs@GO), Nanotechnology, 29 (2018) 015501 - 015508.

[126] C.M. Hangarter, M. Bangar, A. Mulchandani, N.V. Myung, Conducting polymer nanowires for chemiresistive and FET-based bio/chemical sensors, Journal of Materials Chemistry, 20 (2010) 3131 – 3140.

[127] S. Igbal, S. Ahmad, Recent development in hybrid conducting polymers: Synthesis, applications and future prospects, Journal of Industrial and Engineering Chemistry, 60 (2018) 53 – 84.

[128] M.-Y. Chuang, Y.-T. Lin, T.-W. Tung, L.-Y. Chang, H.-W. Zan, H.-F. Meng, C.-T. Lu, Y.-T. Tao, Room-temperature operated organic based acetone gas sensor for breath analysis, Sensors and Actuators B, 260 (2018) 593 – 600.

[129] A. Daneshkhak, S. Shrestha, M. Agarwal, K. Varahramyan, Poly(vinylidene fluoride-hexafluoropropylene) composite sensors for volatile organic compounds detection in breath, Sensors and Actuators B, 221 (2015) 635 – 643.

[130] J.-S. Do, S.-H. Wang, On the sensitivity of conductimetric acetone gas based on polypyrrole and polyaniline conducting polymers, Sensors and Actuators B, 185 (2013) 39 – 46.

[131] T. Sen, S. Mishra, N.G. Shimpi, Synthesis and sensing applications of polyaniline nanocomposites: a review, Royal Science of Chemistry, 6 (2016) 42196 – 42222.

[132] M. Das, D. Sarkar, One-pot synthesis of zinc oxide-polyaniline nanocomposite for fabrication of efficient room temperature ammonia gas sensor, Ceramics International, 43 (2017) 11123 – 11131.

[133] T. Xie, G. Xie, Y. Su, D. Hongfei, Z. Ye, Y. Jiang, Ammonia gas sensors based on poly(3-hexylthiophene)-molybdenum disulphide film transistors, Nanotechnology, 27 (2016) 065502 – 065511.

[134] S.R. Nalage, S.T. Navale, V.B. Patil, Polypyrrole-NiO hybrid nanocomposite: structural, morphological, optical and electrical transport studies, Measurement, 46 (2013) 3268 – 3275.

[135] S.R. Nalage, A.T. Mane, R.C. Pawar, C.S. Lee, V.B. Patil, Polypyrrole-NiO hybrid nanocomposite films: highly selective, sensitive and reproducible NO_2 sensor, Ionics, 20 (2014) 1607 – 1616.

[136] S.R. Nalage, S.T. Navale, R.S. Mane, M. Naushad, F.J. Stadlar, V.B. Patil, Preparation of camphor-sulfonic acid doped PPY-NiO hybrid nanocomposite for detection of toxic nitrogen dioxide, Synthetic Metals, 209 (2015) 426 – 433.

[137] L.L. Noto, S.S. Pitale, O.M. Ntwaeaborwa, J.J. Terblans, H.C. Swart, Cathodoluminescent stability of rare earth tantalate phosphors, Journal of Luminescence, 140 (2013) 14 – 20.

[138] R. Cao, Z. Shi, G. Quan, Z. Hu, G. Zheng, T. Chen, S. Guo, H. Ao, Rare-earth free broadband $Ca_3Mg_3P_4O_{16}$:Mn^{2+} red phosphor: Synthesis and luminescent properties, Journal of Luminescence, 194 (2018) 542 – 546.

[139] V.B. Pawade, H.C. Swart, S.J. Dhoble, Review of rare earth activated blue emission phosphors prepared by combustion synthesis, Renewable and Sustainable Energy Reviews, 52 (2015) 596 – 612.

[140] S.J. Mofokeng, V. Kumar, R.E. Kroon, O.M. Ntwaeaborwa, Structure and optical properties of Dy^{3+} activated sol-gel ZnO-TiO_2 nanocomposites, Journal of Alloys and Compounds, 711 (2017) 121 – 131.

[141] S.V. Motloung, B.F. Dejene, O.M. Ntwaeaborwa, H.C. Swart, R.E. Kroon, Colour tuning and energy transfer pathways in $MgAl_2O_4$ triply doped with 0.1 % Ce^{3+}, 0.1 % Eu^{2+}, x% Tb^{3+} (0 < x < 2%) nanocrystals synthesized using sol-gel process, Chemical Physics, 487 (2017) 75 – 86.

[142] W. Shide, L. Chao, W. Wei, W. Huanxin, S. Yan, Z. Youqi, L. Lingzhen, Nd-doped SnO_2: characterization and its gas sensing property, Journal of Rare Earths, 28 (2010) 171 – 173.

[143] A. Hastir, N. Kohli, R.C. Singh, Comparative study on gas sensing properties of rare earths (Tb, Dy and Er) doped ZnO sensor, Journal of Physics and Chemistry of Solids, 105 (2017) 23 – 34.

[144] H.T. Giang, H.T. Duy, P.Q. Ngan, G.H. Thai, D.T.A. Thu, D.T. Thu, N.N. Toan, Hydrocarbon gas sensing of nanocrystalline perovskite oxides $LnFeO_3$ (Ln = La, Nd, and Sm), Sensors and Actuators B, 158 (2011) 246 – 251.

[145] M. Anbia, S. E. M. Fard, Humidity sensing properties of Ce-doped nanoporous ZnO thin film prepared by sol-gel method, Journal of Rare Earths, 30 (2012) 38 - 42.

[146] X. Dong, X. Cheng, X. Zhang, L. Sbui, Y. Xu, S. Gao, H. Zhao, L. Huo, A novel coral-shaped Dy_2O_3 gas sensor for high sensitivity NH_3 detection at room temperature, Sensors and Actuators B, 255 (2018) 1308 - 1315.

[147] N. Koshizaki, T. Oyama, Sensing characteristic of ZnO-based NOx sensor, Sensors and Actuators B, 66 (2000) 119 – 121.

[148] S. Banno, N. Imanaka, G. Adachi, Selective nitrogen dioxide sensor based on nickel copper oxide mixed with rare earths, Sensors and Actuators B, 24 (1995) 619 – 622.

[149] A. Hastir, N. Kohli, R.C. Singh, Temperature dependent selective and sensitive terbium doped ZnO nanostructures, Sensors and Actuators B, 231 (2016) 110 – 119.

[150] Y. Wang, B. Liu, S. Xiao, H. Li, L. Wang, D. Cai, D. Wang, Y. Liu, Q. Li, T. Wang, High performance and negative temperature coefficient of low temperature hydrogen gas sensors using palladium decorated tungsten oxide, Journal of Materials Chemistry A, 3 (2015) 1317 - 1324.

[151] S.R. Gawali, V.L. Patil, V.G. Deonikar, S.S. Patil, D.R. Patil, P.S. Patil, J. Pant, Ce doped NiO nanoparticles as selective NO_2 gas sensor, Journal of Physics and Chemistry of Solids, 114 (2018) 28 – 35.

[152] A.A. Farghali, M.H. Khedr, S.I. El-Dek, A.E. Megahed, Synthesis and multifunctionality of (CeO_2 - NiO) nanocomposites synthesized via sonochemical technique, Ultrasonics Sonochemistry, 42 (2018) 556 – 566.

[153] C. Mrabet, M.B. Amor, A. Bookhachem, M. Amlouk, T. Manoubi, Physical properties of La-doped NiO sprayed thin films for optoelectronic and sensor applications, Ceramics International, 42 (2016) 5963 – 5978.

[154] X. -Y. Jiang, L. Zhang, Y. -L. Liu, X.-D. Yu, Y.-Y. Liang, P. Qu, W.-W. Zhao, J.-J. Xu, H.-Y. Chen, Hierarchical $CuInS_2$-based heterostructure: Application for photocathodic bioanlysis of sarcosine, Biosensors and Bioelectronics, 107 (2018) 230 - 236.

[155] J.N. Tiwari, R.N. Tiwari, K.S. Kim, Zero-dimensional, one-dimensional, two-dimensional and three-dimensional nanostructured materials for advanced electrochemical energy devices, Progress in Materials Science, 57 (2012) 724 - 803.

[156] H. Jahangiri, A.Y. Lehi, A. Akbari, Hierarchical nanostructures as novel antifouling agents in nanofiltration process, Desalination, 375 (2015) 116 - 120.

[157] H.H. Nersisyan, J.H. Lee, J.-R. Ding, K.-S. Kim, K.V. Manukyan, A.S. Mukasyan, Combustion synthesis of zero-, one-, two- and three-dimensional nanostructures: Current trends and future perspectives, Progress in Energy and Combustion Science, 63 (2017) 79 - 118.

[158] J.P. Cheng, J. Wang, Q.Q. Li, H.G. Liu, Y. Li, A review of recent developments in tin dioxide composites for gas sensing application, Journal of Industrial and Engineering Chemistry, 44 (2016) 1 - 22.

[159] J.-H. Lee, Gas sensors using hierarchical and hollow oxide nanostructures: overview, Sensors and Actuators B, 140 (2009) 319 - 336.

[160] L. Li, C. Zhang, W. Chen, Fabrication of SnO_2-SnO nanocomposites with p-n heterojunctions for the low-temperature sensing of NO_2 gas, Nanoscale, 7 (2015) 12133 - 12133.

[161] D. Ju, H. Xu, H. Gong, Z. Qin, J. Guo, J. Zhang, B. Cao, Direct hydothermal growth of ZnO nanosheets on electrode for ethanol sensing, Sensors and Actuators B, 215 (2015) 39 – 46.

[162] C. Liu, L. Zhao, B. Wang, P. Sun, Q. Wang, Y. Gao, X. Liang, T. Zhang, G. Lu, Acetone gas sensor based on NiO/ZnO hollow spheres: Fast response and recovery, and low (ppb) detection limit, Journal of Colloid and Interface Science, 495 (2017) 207 – 215.

[163] A. Mirzaei, G.-J. Sun, J.K. Lee, C. Lee, S. Choi, H.W. Kim, Hydrogen sensing properties and mechanism of $NiO-Nb_2O_5$ composite nanoparticle-based electrical gas sensors, Ceramics International, 43 (2017) 5247 – 5254.

[164] S. Bai, Y. Tian, Y. Zhao, H. Fu, P. Tang, R. Luo, D. Li, A. Chen, C.C. Liu, Construction of $NiO@ZnSnO_3$ hierarchical microspheres decorated with NiO nanosheets for formaldehyde sensing, Sensors and Actuators B, 259 (2018) 908 – 916.

[165] T.-H. Kim, C.-H. Kwak, J.-H. Lee, $NiO/NiWO_4$ composite yolk-shell spheres with nanoscale NiO outer layer for ultrasensitive and selective detection of subppm level p-xylene, ACS Materials & Interfaces, 9 (2017) 32034 – 32043.

[166] X. Chen, C.K.Y. Wong, C.A. Yuan, G. Zhang, Nanowire-based gas sensors, Sensors and Actuators B, 177 (2013) 178 – 195.

[167] J.-H. Park, M.-S. Cho, D. Lim, J.-G. Park, SnO_2 nanowire gas sensor operating at room temperature, Journal of Nanoscience and Nanotechnology, 14 (2014) 8038 – 8042.

[168] G.-J. Sun, H. Kheel, S. Park, S. Lee, S.E. Park, C. Lee, Synthesis of TiO_2 nanorods decorated with NiO nanoparticles and their acetone sensing properties, Ceramics International, 42 (2016) 1063 – 1069.

[169] Y. Zheng, J. Wang, P. Yao, Formaldehyde sensing properties of electrospun NiO-doped SnO_2 nanofibers, Sensors and Actuators B, 156 (2011) 723 – 730.

[170] L. Xu, R. Zheng, S. Liu, J. Song, J. Chen, B. Dong, H. Song, NiO@ZnO heterostructured nanotubes: coelectrospinning fabrication, characterization, and highly enhanced gas sensing, Inorganic Chemistry, 51 (2012) 7733 – 7740.

[171] C. Li, C. Feng, F. Qu, J. Liu, L. Zhu, Y. Liu, Y. Wang, F. Li, J. Zhou, S. Ruan, Electrospun nanofibers of p-type NiO/n-type ZnO heterojunction with different NiO content and its influence on trimethylamine sensing properties, Sensors and Actuators B, 207 (2015) 90 – 96.

[172] Y. Wang, H. Zhang, X. Sun, Electrospun nanowebs of NiO/SnO_2 pn heterojunctions for enhanced gas sensing, Applied Surface Science, 389 (2016) 514 – 520.

[173] C. Baratto, R. Kumar, E. Comini, M. Ferroni, M. Campanini, Bottle brush shaped heterostuctures of NiO-ZnO nanowires: growth study and sensing properties, Nanotechnology, 28 (2017) 465502 – 465508.

[174] Z. Wang, Z. Li, J. Shun, H. Zheng, W. Wang, W. Zheng, C. Wang, Improved hydrogen monitoring properties based on p-NiO/n-SnO_2 heterojunction composite nanofibers, The Journal of Physical Chemistry C, 114 (2010) 6100 – 6105.

[175] J. Zhang, H. Lu, C. Liu, C. Chen, X. Xin, Porous NiO-WO_3 heterojunction nanofibers fabricated by electrospinning with enhanced gas sensing properties, Royal Society of Chemistry Advances, 7 (2017) 40499 – 40509.

[176] M.U. Haq, Z. Wen, Z. Zhang, S. Khan, Z. Lou, Z. Ye, L. Zhu, Scientific Reports, 8 (2018) 1705 – 1717.

[177] C. Yan, H. Lu, J. Gao, G. Zhu, F. Yin, Z. Yang, Q. Liu, Synthesis of porous NiO-In_2O_3 composite nanofibers by electrospinning and their highly enhanced gas sensing properties, Journal of Alloys and Compounds, 699 (2017) 567 – 574.

[178] S.G. Leonardi, Two-dimensional zinc oxide nanostructures for gas sensor applications, Chemosensors, 5 (2017) 17 – 45.

[179] L. Li, C. Zhang, R. Zhang, X. Gao, S. He, M. Liu, X. Li, W. Chen, 2D ultrathin Co_3O_4 nanosheet array deposited on 3D carbon foam for enhanced ethanol gas sensing application, Sensors and Actuators B, 244 (2017) 664 – 672.

[180] Z. Qiu, K. Xu, H. Yue, H. Wang, J. Zhang, C. Ouyanga, C. Xie, D. Zheng, Enhanced room temperature NH_3 gas sensing by 2D SnS_2 with sulphur vacancies synthesized by chemical exfoliation, Sensors and Actuators B, 262 (2018) 771 – 779.

[181] V. Shukla, J. Warna, N.K. Jena, A. Grigoriev, R. Ahuja, Toward the realization of 2D borophene based gas sensor, The Journal of Physical Chemistry C, 121 (2017) 26869 – 26876.

[182] W. Yang, L. Gan, H. Li, T. Zhai, Two-dimensional layered nanomaterials for gas sensing applications, Inorganic Chemistry Frontiers, 3 (2016) 433 – 451.

[183] X. Zhou, X. Cheng, Y. Zhu, A.A. Elzatahry, A. Alghamdi, Y. Deng, D. Zhao, Ordered porous metal oxide semiconductors for gas sensing, Chinese Chemical Letters, 29 (2018) 405 – 416.

[184] M. Tonezzer, L.T.T. Dang, H.Q. Tran, S. Iannotta, Multiselective visual gas sensor using nickel oxide nanowires as chemiresistor, Sensors and Actuators B, 255 (2018) 2785 – 2793.

[185] E.D. Gaspera, M. Guglielmi, S. Agnoli, G. Granozzi, M.L. Post, V. Bello, G. Mattei, A. Martucci, Au nanoparticles in nanocrystalline TiO_2-NiO films for SPR-based, selective H_2S gas sensing, Chemistry of Materials, 22 (2010) 3407 – 3417.

[186] M. Kaur, B.K. Dadhich, R. Singh, K. Ganapathi, T. Bagwaiya, S. Bhattacharya, A.K. Debnath, K.P. Muthe, S.C. Gadkari, RF sputtered SnO_2:NiO thin films as sub-ppm H_2S sensor operable at room temperature, Sensors and Actuators B, 242 (2017) 389 – 403.

[187] C. Bourgeois, P. Dufour, J.C. Mutin, A. Steinbrunn, An electrical conductivity and TEM study of the sulphurization by gaseous H_2S of NiO single crystals, Journal of Materials Science, 17 (1982) 2298 – 2308.

[188] J. Fang, Y. Zhu, D. Wu, C. Zhang, S. Xu, D. Xiong, P. Yang, L. Wang, P.K Chu, Gas sensing properties of NiO/SnO$_2$ heterojunction thin film, Sensors and Actuators B, 252 (2017) 1163 – 1168.

[189] A. Kumar, A. Sanger, A. Kumar, R. Chandra, Fast response ammonia sensors based on TiO$_2$ and NiO nanostructured bilayer thin films, Royal Society of Chemistry, 6 (2016) 77636 – 77643.

[190] J. Guo, J. Zhang, H. Gong, D. Ju, B. Cao, Au nanoparticle-functionalized 3D SnO$_2$ microstructures for high performance gas sensor, Sensors and Actuators B, 226 (2016) 266 -272.

[191] T.-K. Tseng, J. Choi, D.-W. Jung, M. Davidson, P.H. Holloway, Three-dimensional self-assembled hierarchical architectures of gamma-phase flowerlike bismuth oxide, ACS Applied Materials Interface, 2 (2010) 943 – 946.

[192] B.-Y. Kim, J.H. Ahn, J.-W. Yoon, C. –S. Lee, Y.C. Kang, F. Abde, A.A. Wazzan, J. –H. Lee, Highly selective xylene sensor based on NiO/NiMoO$_4$ nanocomposite hierarchical spheres for indoor air monitoring, ACS Applied Materials Interfaces, 8 (2016) 34603 – 34611.

[193] C. Liu, B. Wang, T. Liu, P. Sun, Y. Gao, F. Liu, G. Lu, Facile synthesis and gas sensing properties of the flower-like NiO-decorated ZnO microstructures, Sensors and Actuators B, 235 (2016) 294 – 301.

[194] A.K. Nayak, R. Ghosh, S. Santra, P.K. Guha, D. Pradhan, Hierarchical nanostructured WO$_3$-SnO$_2$ for selective sensing of volatile organic compounds, Nanoscale, 7 (2015) 12460.

[195] G.-J. Sun, H. Kheel, J.K. Lee, S. Choi, S. Lee, C. Lee, H$_2$S gas sensing properties of Fe$_2$O$_3$ nanoparticle-decorated NiO nanoplate sensors, Surface & Coatings Technology, 307 (2016) 1088 – 1095.

[196] Z. Qu, Y. Fu, B. Yu, P. Deng, L. Xing, X. Xue, High and fast H$_2$S response of NiO/ZnO nanowire nanogenerator as a self-powered gas sensor, Sensors and Actuators B, 222 (2016) 78 – 86.

[197] X. Li, Z. Mu, J. Hu, Z. Cui, Gas sensing characteristics of composite NiO/Al_2O_3 for 2-chloroethanol at low temperature, Sensors and Actuators B, 232 (2016) 143 – 149.

[198] J. Zhang, J. Wu, X. Wang, D. Zheng, C. Xie, Enhancing room temperature NO_2 sensing properties via forming heterojunction for NiO-rGO composited with SnO_2 nanoplates, Sensors and Actuators B, 243 (2017) 1010 – 1019.

[199] H. Xu, J. Zhang, A.U. Rehman, L. Gong, K. Kan, L. Li, Synthesis of NiO@CuO nanocomposite as high-performance gas sensing material for NO_2 at room temperature, Applied Surface Science, 412 (2017) 230 – 237.

[200] C. Balamurugan, Y.J. Jeong, D.W. Lee, Enhanced H_2S sensing performance of a p-type semiconducting PdO-NiO nanoscale heteromixture, Applied Surface Science, 420 (2017) 638 – 650.

[201] Y. Lu, Y. Ma, S. Ma, S. Yan, Hierarchical heterostructure of porous NiO nanosheets on flower-like ZnO assembled by hexagonal nanorods for high-performance gas sensor, Ceramics International, 43 (2017) 7508 – 7515.

[202] J.-K. Wang, K.T. Liao, W.J. Tseng, NiO/SnO_2 hybrid nanowires for enhanced NO_2 gas sensing, Ceramics International, 43 (2017) S541 – S546.

[203] P. Tyagi, A. Sharma, M. Tomar, V. Gupta, SnO_2 thin film sensor having NiO catalyst for detection of SO_2 gas with improved response characteristics, Sensors and Actuators B, 248 (2017) 998 – 1005.

[204] S. Bai, J. Liu, J. Guo, R. Luo, D. Li, Y. Song, C.C. Liu, A. Chen, Facile preparation of SnO_2/NiO composites and enhancement of sensing performance to NO_2, Sensors and Actuators B, 249 (2017) 22 – 29.

[205] M. Yang, X. Zhang, X. Cheng, Y. Xu, S. Gao, H. Zhao, L. Huo, Hierarchical NiO cube/nitrogen doped reduced graphene oxide composite with enhanced H_2S sensing properties at low temperature, ACS Applied Materials & Interfaces, 9 (2017) 26293 – 26303.

[206] L. Zhu, W. Zeng, J. Yang, Y. Li, Fabrication of hierarchical hollow NiO/ZnO microspheres for ethanol sensing property, Materials Letters, 230 (2018) 297 – 299.

86

[207] J. Hu, J. Yang, W. Wang, Y. Xue, Y. Sun, P. Li, K. Lian, W. Zhang, L. Chen, J. Shi, Y. Chen, Synthesis and gas sensing properties of NiO/SnO_2 hierarchical structures toward ppb-level acetone detection, Materials Research Bulletin, 102 (2018) 294 – 303.

[208] S. Zhang, G. Sun, Y. Li, B. Zhang, L. Lin, Y. Wang, J. Cao, Z. Zhang, Continuously improved gas sensing performance of SnO_2/Zn_2SnO_4 porous cubes by structure evolution and further NiO decoration, Sensors and Actuators B, 255 (2018) 2936 – 2943.

[209] L. Zhu, W. Zeng, J. Yang, Y. Li, One-step hydrothermal fabrication of nanosheet-assembled NiO/ZnO microflower and its ethanol sensing property, Ceramics International, 44 (2018) 19825 – 19830.

[210] H. Gao, L. Zhao, L. Wang, P. Sun, H. Lu, F. Liu, X. Chuai, G. Lu, Ultrasensitive and low detection limit of toluene gas sensor based on SnO_2-decorated NiO nanostructure, Sensors and Actuators B, 255 (2018) 3505 – 3515.

[211] W. Tan, J. Tan, L. Fan, Z. Yu, J. Qian, X. Huang, Fe_2O_3-loaded NiO nanosheets for fast response/recovery and high response gas sensor, Sensors and Actuators B, 256 (2018) 282 – 293.

[212] J. Zhang, D. Hu, S. Tian, Z. Qin, D. Zeng, C. Xie, $CuInS_2$ QDs decorated ring-like NiO for significantly enhanced room temperature NO_2 sensing performances via effective interfacial charge transfer, Sensors and Actuators B, 256 (2018) 1001 – 1010.

[213] J.-H. Kim, J.-H. Lee, A. Mirzaei, H.W. Kim, S.S. Kim, SnO_2 (n) - NiO (p) composite nanowebs: Gas sensing properties and sensing mechanisms, Sensors and Actuators B, 258 (2018) 204 – 214.

[214] N. Kaur, D. Zappa, M. Ferroni, N. Poli, M. Campanini, P. Negrea, E. Comini, Branch-like NiO/ZnO heterostructures for VOC sensing, Sensors and Actuators B, 262 (2018) 477 – 485.

[215] H. Ren, C. Gu, S.W. Joo, J. Zhao, Y. Sun, Effective hydrogen gas sensor based on NiO@rGO nanocomposite, Sensors and Actuators B, 266 (2018) 506 – 513.

[216] D. Meng, D. Liu, G.Wang, Y. Shen, X. San, M. Li, F. Meng, Low-temperature formaldehyde gas sensors based on $NiO-SnO_2$ heterojunction microflowers assembled by thin porous nanosheets, Sensors and Actuators B, 273 (2018) 418 – 428.

[217] X. San, M. Li, D. Liu, G. Wang, Y. Shen, D. Meng, A facile one-step hydrothermal synthesis of NiO/ZnO heterojunction microflowers for the enhanced formaldehyde sensing properties, Journal of Alloys and Compounds, 739 (2018) 260 – 269.

[218] J.M. Walker, S.A. Akbar, P.A. Morris, Synergistic effects in gas sensing semiconducting oxide nano-heterostructures: A review, Sensors and Actuators B, 286 (2019) 624 – 640.

[219] D. Wu, W. Li, A. Rai, X. Wu, H.C.P. Movva, M.N. Yogeesh, Z. Chu, S.K. Banerjee, D. Akinwande, K. Lai, visualization of local conductance in MoS_2/WSe_2 heterostructure transistors, Nano letters, 19 (2019) 1976 – 1981.

<u>Highlights:</u>

- Reviewing various synthesis methods NiO for gas sensing.

- Discuss effects of various metals such as transition metal dichalcogenide, etc.

- Provides influence of 0D-3D heterostructures on NiO gas sensing characteristics

- The arrangement of various SMO to form heterostructures is discussed

- Show that number of publications on NiO based heterostructures increased since the year 2010.